Reversal of RNA toxicity in myotonic dystrophy via a decoy RNA-binding protein with high affinity for expanded CUG repeats

Ludovic Arandel, Magdalena Matloka, Arnaud F Klein, Frédérique Rau, Alain Sureau, Michel Ney, Aurélien Cordier, Maria Kondili, Micaela Polay-Espinoza, Naira Naouar, et al.

Reversal of RNA toxicity in myotonic dystrophy via a decoy RNA-binding protein with high affinity for expanded CUG repeats

Ludovic Arandel[1,&], Magdalena Matloka[1,&], Arnaud F. Klein[1], Frédérique Rau[1], Alain Sureau[1], Michel Ney[1], Aurélien Cordier[1], Maria Kondili[1], Micaela Polay-Espinoza[1], Naira Naouar[1], Arnaud Ferry[1,3], Mégane Lemaitre[1,4], Séverine Begard[2], Morvane Colin[2], Chloé Lamarre[2], Hélène Tran[2], Luc Buée[2], Joëlle Marie[1], Nicolas Sergeant[2*] & Denis Furling[1*]

[1]Sorbonne Université, Inserm, Institut de Myologie, Centre de Recherche en Myologie, 75013 Paris, France
[2]Université de Lille, Inserm, CHU Lille, Lille Neuroscience & Cognition, 59045 Lille, France
[3]Sorbonne Paris Cité, Université Paris Descartes, 75005 Paris, France
[4]Sorbonne Université, Inserm, Phénotypage du petit animal, 75013 Paris, France

[&]These authors contributed equally
*Corresponding authors, nicolas.sergeant@inserm.fr; denis.furling@sorbonne-universite.fr

Myotonic dystrophy type 1 (DM1) is an RNA-dominant disease whose pathogenesis stems from the functional loss of muscleblind-like RNA-binding proteins (RBPs), which causes the formation of alternative-splicing defects. The loss of functional muscleblind-like protein 1 (MBNL1) results from its nuclear sequestration by mutant transcripts containing pathogenic expanded CUG repeats (CUGexp). Here we show that an RBP engineered to act as a decoy for CUGexp reverses the toxicity of the mutant transcripts. In vitro, the binding of the RBP decoy to CUGexp in immortalized muscle cells derived from a patient with DM1 released sequestered endogenous MBNL1 from nuclear RNA foci, restored MBNL1 activity, and corrected the transcriptomic signature of DM1. In mice with DM1, the local or systemic delivery of the RBP decoy via an adeno-associated virus into the animals' skeletal muscle led to the long-lasting correction of the splicing defects and to ameliorated disease pathology. Our findings support the development of decoy RBPs with high binding affinities for expanded RNA repeats as a therapeutic strategy for myotonic dystrophies.

One-sentence editorial summary (to appear right below the title of your Article on the journal's website):
RNA-binding proteins acting as decoys for pathogenic expanded CUG RNA repeats reverse the toxicity of the mutant transcripts in muscle cells derived from a patient with myotonic dystrophy type 1 and in a mouse model of the disease.

RNA-binding proteins (RBPs) play a key role in the regulation of RNA processing, and the disruption of their activities is responsible for a growing number of diseases[1]. Thus, functional loss of Muscleblind-like (MBNL) RBPs that regulate alternative splicing events during the developmental transition from fetal to adult isoforms, represents a central pathophysiologic mechanism of myotonic dystrophy type 1 (DM1) disease[2,3]. DM1, one of the most common form of muscular dystrophy in adults, is caused by expanded CTGn repeats (n>50) located in the 3'UTR of the *DMPK* gene[4]. Mutant *DMPK* transcripts containing expanded CUG repeats (CUGexp) are retained in the nucleus as discrete ribonucleoprotein foci[5]. Due to its high affinity for YGCY RNA motifs[6], MBNL1 is sequestered by nuclear CUGexp-RNA foci in DM1 muscle cells leading to its functional loss, alternative splicing misregulations and ultimately, muscle impairment. Consistently, *Mbnl* deficient mice display major splicing changes characteristic for advanced DM1 disease and cardinal features including myotonia, muscle weakness, heart defects and reduced lifespan[7]. Among MBNL1-dependent splicing events that are misregulated in striated muscles of DM1 patients[8], alterations of *CLCN1, INSR, BIN1, DMD* and *SCN5A* pre-mRNAs are associated with myotonia, insulin resistance, muscle weakness, dystrophic process and cardiac conduction defects respectively, all symptoms of DM1[9,10,11,12,13].

Therapeutic strategies for this RNA dominant disease aim to target mutant CUGexp-RNAs either by inducing their degradation or by interfering with the deleterious CUGexp:MBNL1 interaction. All RNA-based approaches that have shown promising beneficial effects in DM1 models including antisense oligonucleotides[14,15,16] small compounds[17,18,19,20] and RNA-targeting Cas system[21,22,23], share a common feature: the release of sequestered MBNL1 from CUGexp-RNA foci that underlies the recovery of MBNL1 activity and the correction of DM1-associated phenotypes. Moreover, overexpressing MBNL1 in skeletal muscles of DM1 mice using local injection of recombinant adeno-associated viral (AAV) vectors corrects both splicing defects and myotonia confirming that CUGexp-RNA toxicity is largely mediated by a MBNL1 loss-of-function mechanism[24]. However, systemic AAV-mediated delivery of MBNL1 proteins or derivates[25] has not been considered for clinical development so far.

Although restoration of MBNL functions in cells expressing CUGexp-RNA represents a valuable strategy for therapeutic intervention in DM1, the overexpression of a single MBNL isoform could be a challenging approach regarding activities of the various MBNL paralog isoforms and their fine-tuned expression. Indeed, MBNL RBP family is composed of three paralogs (*MBNL1, MBNL2, MBNL3*) and up to ten isoforms per paralog that are highly regulated in both developmental and cell/tissue-specific manners[26]. While MBNL1 is the major isoform expressed in striated muscle, MBNL2 and MBNL3 are predominantly expressed in central nervous system and placenta, respectively[27]. All MBNL proteins can bind to CUGexp and can be sequestered into nuclear RNA foci[28] resulting in altered function of specific paralog products according to the expression of *CUGexp-DMPK* transcripts among tissues. Whereas loss of MBNL function is deleterious, inappropriate expression of MBNL should also be carefully taken into consideration as pointed out by the overexpression of MBNL1 that leads to additional cognitive alterations in MBNL2 deficient mice[29] and either improvement or worsening of muscle phenotypes in DM1[30,31].

In this study, we investigated a decoy-based strategy[32] in which an engineered RBP could act as a CUGexp-decoy by competing for CUGexp binding to release functional endogenous MBNL1 from RNA foci. For this purpose, we modified MBNL1 itself and engineered a MBNL1Δ-decoy that still has a high CUGexp binding affinity but reduced splicing activity. We showed that the expression of MBNL1Δ-decoy in muscle cells derived from a DM1 patient reverses misregulated splicing events and improves the disease transcriptomic signature. We demonstrated that the action of the decoy is triggered by its binding to CUGexp allowing the displacement of MBNL1 from RNA foci and the recovery of functional endogenous MBNL1 in DM1 cells. Moreover, CUGexp-RNA foci formed by MBNL1Δ-decoy are less stable resulting in a significant reduction in their number as well as CUGexp-RNA levels. In addition, expression of MBNL1Δ-decoy in skeletal muscles of WT mice using AAV vectors showed no changes at histologic levels and limited effect on direct MBNL1 targets or transcripts containing short CUG repeats. In the DM1 HSA^{LR} mouse model, a single intramuscular or systemic administration of AAV-MBNL1Δ-decoy resulted in an efficient and long-term correction of muscular DM1-associated phenotypes including splicing defects, myopathy and myotonia. Our results strongly support the concept of a decoy gene therapy based on engineered RNA-binding proteins with high CUGexp-binding affinities as a therapeutic avenue for DM1.

Results

Engineered RBP with CUGexp binding affinity and decoy activity. To develop a decoy-strategy based on an engineered RBP with a high affinity for expanded CUG repeats, we took advantage of the binding of MBNL1 itself to CUGexp that is provided by two tandem zing finger (ZnF) domains located at the N-terminal part of the protein. We engineered a truncated MBNL1 protein (referred here as MBNL1Δ) that keeps the ZnF domains required for the binding to YGCY RNA motifs but lacks the C-terminal domain implicated in

splicing activity, cellular localization and oligomerization[33] (**Fig. 1A**). Splicing assay performed in HeLa cells by co-transfecting plasmids containing either MBNL1Δ or MBNL1 and *cTNT* or *IR* minigenes confirmed that MBNL1Δ has a reduced splicing activity when compared to MBNL1, as previously described[33,34] (**Supplementary Fig. 1A**). Furthermore, co-transfection experiments in HeLa cells expressing a construct bearing 960 CTG showed that GFP-MBNL1Δ colocalizes with nuclear CUGexp-RNA foci like GFP-MBNL1 itself (**Fig. 1B**). Because the binding affinity to CUG repeats is similar between MBNL1Δ and MBNL1 (**Supplementary Fig. 1B**) as shown for other YGCY RNA motifs[33,35], we tested whether MBNL1Δ could compete with MBNL1 for binding to P^{32}-labelled CUGexp. *In vitro* competition assay demonstrated that increasing amount of MBNL1Δ or MBNL1 displace MBNL1 or MBNL1Δ respectively from CUGexp in a dose dependent manner (**Fig. 1C)** indicating that both proteins can compete for CUGexp binding. From these *in vitro* results, we hypothesized that MBNL1Δ could act as a CUGexp-competitive decoy to promote the release of endogenous MBNL1 from RNA foci and the recovery of a functional pool of endogenous MBNL1 in DM1 cells.

MBNL1Δ-decoy reverses CUGexp-RNA toxicity in DM1 patient-derived muscle cells. To test whether MBNL1Δ-decoy can restore endogenous MBNL1 activity in DM1 muscle cells, misspliced alternative events regulated by MBNL1 were used as biomarker of functional MBNL1 recovery[8,36]. For this purpose, DM1 patient-derived muscle cells displaying molecular disease-associated phenotypes[37] were transduced with a lentiviral vector containing a Tet-On GFP-tagged MBNL1Δ construct allowing its expression only in the presence of doxycycline (**Fig. 1D**, upper panel**)**. Without doxycycline, differentiated DM1 muscle cells displayed splicing misregulations of *DMD exon 78*, *MBNL1 exon 5, NFIX exon 7*, *MBNL2 exon 5* and *ATP2A1 exon 22* pre-mRNAs compared to differentiated WT muscle cells (**Fig. 1E** and **Supplementary Fig. 2**). Remarkably, these splicing defects were corrected by MBNL1Δ expression after doxycycline induction suggesting a recovery of functional MBNL1 in MBNL1Δ-treated DM1 muscle cells. Transcriptomic analysis following global RNA sequencing confirmed that the vast majority of misregulated splicing events (81%) measured in differentiated DM1 muscles cells are normalized (>80% of correction) or partially corrected (between 20 to 80%) by MBNL1Δ, with a mean level of splicing correction of 72% (**Fig. 1F,** upper panel and **Supplementary Table 1**). However, the reversal by MBNL1Δ of each pathological alternative splicing event that are abnormally excluded (61%) or included (39%) did not significantly correlate with the severity of the DM1-mediated splicing event (R^2: 0.003; P-value: 0.18 and R^2: 0.0036; P-value: 0.079, respectively). At the gene expression level, 72% of the transcripts that are deregulated in differentiated DM1 muscle cells are normalized or partially corrected by MBNL1Δ, with a mean level of correction of 56% (**Fig. 1F**, lower panel and **Supplementary Table 2**). Gene Ontology (GO) analysis of gene expression and alternative splicing showed that the genes that undergo correction as well as uncorrected genes were distributed uniformly, with no significant enrichment across the major biological processes that are deregulated in DM1 muscles cells (**Supplementary Fig. 3)**. Altogether, these results indicated that the overall transcriptome of differentiated DM1 muscle cells is significantly improved by the expression of MBNL1Δ.

MBNL1Δ-decoy action requires the recovery of endogenous MBNL1 activity. To ascertain that the action of MBNL1Δ-decoy is mediated by the recovery of functional endogenous MBNL activity, the expression of *MBNL1* and *MBNL2* mRNAs was silenced in WT or DM1 muscle cells expressing or not MBNL1Δ (**Fig. 1D**, upper panel**)**. Transfection of specific siRNA directed against *MBNL1* and *MBNL2* mRNAs induced a significant reduction in the level of *MBNL1* and *MBNL2* transcripts (50% and 70%, respectively), which was confirmed by reduced levels of MBNL1 and MBNL2 proteins (**Supplementary Fig. 4A-B**). As expected, dual *MBNL1/MBNL2* mRNA silencing in WT cells led to splicing changes of *DMD exon 78*, *MBNL1 exon 5, NFIX exon 7*, *TNNT2 exon 5*, *LDB3 exon 11* and *SOS1 exon 25* pre-mRNAs similar to those found in DM1 cells (**Fig**. **1G** and **Supplementary Fig. 5**). Splicing changes triggered by *MBNL1/MBNL2*-silencing in WT cells were not corrected by the expression of MBNL1Δ indicating that the residual splicing activity of MBNL1Δ did not compensate for MBNL1/MBNL2 deficiency. Also, MBNL1Δ expression did not modify the alternative splicing profiles in WT muscle cells (**Fig**. **1G** and **Supplementary Fig. 5**). In contrast, corrections of splicing misregulations of *DMD, MBNL1, NFIX, TNNT2*, *LDB3* and *SOS1* pre-mRNAs in DM1 cells expressing MBNL1Δ were abolished by *MBNL1/MBNL2* silencing. These data demonstrated that endogenous MBNL1 is required for MBNL1Δ correcting effect supporting a decoy mechanism that releases endogenous MBNL1 from CUGexp to restore a pool of functional MBNL1 in DM1 cells.

MBNL1Δ-decoy interferes with CUGexp-RNA foci dynamics. To assess the effect of MBNL1Δ on pathologic CUGexp:MBNL1 interaction within nuclear RNA foci of DM1 cells, the behavior of RNA foci and sequestered MBNL1 proteins were examined for 8 hours after GFP-MBNL1Δ induction (**Fig. 2A).** In non-treated differentiated DM1 muscle cells, MBNL1 colocalized with nuclear CUGexp-RNA foci (**Fig. 2B** and **Supplementary Fig. 6)**. Following dox-induction in DM1 cells, the expression of MBNL1Δ increased

progressively from 2 to 8 hours (**Fig. 2C**) and a colocalization of MBNL1Δ with the RNA foci was observed (**Fig. 2B** and **Supplementary Fig. 6**). In parallel, the mean number of CUGexp-RNA foci per nucleus significantly decreased from 17 in untreated DM1 cells to 4 in DM1 cells expressing MBNL1Δ for 8 hours (**Fig. 2D**). Northern blot analysis confirmed the reduction of *CUGexp-DMPK* mRNA levels in MBNL1Δ-treated DM1 cells (**Fig. 2E and 2F**). Additionally, the mean intensity of MBNL1 per RNA foci was significantly reduced in MBNL1Δ-expressing DM1 cells compared to untreated DM1 cells (**Fig. 2G).** In association with the reduced number of RNA foci in MBNL1Δ-expressing DM1 cells, an overall 80% reduction of sequestered MBNL1 per nucleus was measured (**Fig. 2H**). Concomitantly, the release of free MBNL1 from RNA foci was associated with its relocalization within the nucleoplasm of MBNL1Δ-treated DM1 cells when compared to untreated DM1 cells (**Fig. 2B** and **Supplementary Fig. 6**). The progressive correction of MBNL1-dependent splicing defects measured in treated DM1 muscle cells confirmed the recovery of a pool of functional MBNL1 following MBNL1Δ treatment (**Fig. 2I-J** and **Supplementary Fig. 7**). Altogether, these results further supported a decoy mechanism in which the competition of MBNL1Δ with MBNL1 for CUGexp-binding favors the release of sequestered MBNL1 and unexpectedly, interferes with the dynamic of CUGexp-RNA foci resulting in reduced steady-state levels of *CUGexp-DMPK* transcripts. As a consequence, sufficient endogenous MBNL1 activity is recovered to reverse molecular DM1-associated phenotypes in patient cells.

MBNL1Δ-decoy forms less stable CUGexp-RNA aggregates than MBNL1. To further define the mechanism through which MBNL1Δ-decoy reduces the number of CUGexp-RNA foci, we first examined the behavior of MBNL1Δ in these foci. FRAP experiments performed in DM1 cells expressing either GFP-tagged MBNL or MBNL1Δ proteins showed that MBNL1Δ-decoy has an increased half-time of recovery in bleached CUGexp-RNA foci and a higher fraction of mobile molecules compared to MBNL1 (**Fig. 3A-D**). Thereby, the presence of the C-terminal part of MBNL1 that is entirely lacking in MBNL1Δ increases fractions of immobile molecules supporting the hypothesis that CUGexp-RNA foci formed by MBNL1Δ-decoy behave differently than their counterparts formed by MBNL1. To assess the effects of MBNL1Δ-decoy on RNA foci formation and stability, we tested whether MBNL1 and MBNL1Δ proteins modulate CUG RNA repeats assembly into large spherical clusters or droplets by liquid-liquid phase separation (LLPS). For this purpose, the behavior of the droplets formed *in vitro* by the fluorescently labeled (CUG)46 RNA repeats was monitored in the absence or presence of purified recombinant MBNL1 or MBNL1Δ proteins (**Fig. 3F**). As shown previously[38], RNAs containing 46 CUG repeats form round-shaped-like droplets with highly dynamic motility, freely moving in solution (**Fig. 3G** and **Supplementary Video 1**). By adding purified MBNL1 protein, the number of RNA-like droplets is dramatically enhanced and their shape changed, promoting formation of elongated and filamentous-like structures (**Fig. 3H**). Neither GST nor RUVBL2 purified proteins had a similar effect (**Supplementary Fig. 8**). Interestingly, CUGexp-RNA/MBNL1 condensates became much more static and fell very quickly onto the glass chamber compared to CUGexp-RNA alone (**Supplementary Video 2**). In contrast, addition of MBNL1Δ led to the formation of more round shaped droplets with less branched like-filamentous structures than those formed with MBNL1and with higher mobility (**Fig. 3G** and **Supplementary Video 3**). The immobile fraction of condensates arising from CUGexp-RNA and MBNL1Δ-decoy increases progressively from 12% at 0.5h to 63% after 8h whereas 69% of CUGexp-RNA/MBNL1 condensates are already motionless at 0.5h and up to 92% after 8h indicating that the composition of droplets influences their biophysical properties (**Fig. 3H**). More strikingly, the number and the size of RNA-like droplets formed by MBNL1Δ are significantly reduced compared to those formed by MBNL1 (**Fig. 3I-J**). Although MBNL1 and MBNL1Δ have the ability to bind CUG repeats, MBNL1Δ-decoy is less prone to form or undergo phase separation condensates with CUGexp-RNA than MBNL1. These results suggested that the C-terminal part of MBNL1 promotes aggregation and stabilization of CUGexp-RNA. Its removal in MBNL1Δ-decoy contributes to form more dynamic or less stable RNA foci, and therefore reduce levels of CUGexp-transcripts measured after MBNL1Δ treatment.

Effect of AAV-mediated MBNL1Δ expression in skeletal muscle of WT mice. To translate our decoy strategy *in vivo*, GFP-tagged MBNL1Δ construct was packaged into a recombinant AAV9 vector ensuring efficient transduction and transgene-delivery in skeletal muscles[39]. As a first step, *Gastrocnemius* muscles of wild-type (WT) mice were injected intramuscularly with AAV-GFP-MBNL1Δ or AAV-GFP vectors ($1x10^{11}$ vg) whereas contralateral muscles received saline vehicle **(Fig. 4A)**. Five weeks later, AAV-GFP-MBNL1Δ or AAV-GFP injected muscles showed no histological changes compared to saline condition **(Fig. 4B-C)**. In contrast, injection of AAV-GFP-MBNL1 vectors ($1x10^{11}$ vg) that reverse splicing misregulation in DM1 HSA^{LR} mice[24] (**Extended Data Fig. 1A),** led to muscle damage in WT mice as revealed by the presence of fibers with internal nuclei (**Fig. 4B-C**). Muscle degeneration/regeneration process was observed two and three weeks after AAV-GFP-MBNL1 injection and confirmed by the re-expression of early markers of myogenesis such as MyoG and Myh8 transcripts (**Extended Data Fig. 1B-C**). Such alterations were not observed in WT muscles injected with MBNL1Δ and ectopic expression of MBNL1Δ did not affect endogenous MBNL1 levels

compared to saline or AAV-GFP injected muscles (**Fig. 4D** and **Extended Data Fig. 2A)**. Moreover, splicing profiles of a panel of genes[8,40] that are abnormally spliced in DM1 and regulated by MBNL1 were not altered in WT muscles expressing either GFP-MBNL1Δ or GFP alone (**Fig. 4E** and **Extended Data Fig. 2B-C**) as shown by a composite splicing index derived from the splicing events (**Fig. 4F**)**.** To examine further effects of MBNL1Δ, RNA-sequencing was performed on muscles samples from WT mice injected with AAV-GFP-MBNL1Δ-decoy, AAV-GFP or saline. Analysis of alternative splicing (adj p-value<0.05; |ΔPsi|>0.2) showed that only few splicing events affecting 12 genes were modified by MBNL1Δ-decoy (**Supplementary Table 3**). Among them, two were also modulated in AAV-GFP-treated muscles in which 11 misspliced events were identified (**Supplementary Table 3**), and two were found deregulated in muscles of MBNL1$^{-/-}$:MBNL2$^{-/+}$ mice in which 970 events were identified[40]. Global gene expression analysis showed that changes (adj p-value<0.05; |Log2FC|>1) induced by AAV-GFP-MBNL1Δ are restricted compared to AAV-GFP (**Fig. 4G**). Moreover, the number of transcripts identified by CLIP as direct MBNL1 targets[41] and CUG-rich transcripts containing tracts of CUG repeats (≥7) that are deregulated in AAV-GFP-MBNL1Δ injected muscles (40 and 18, respectively), were not increased when compared to AAV-GFP injected muscles (57 and 27, respectively). GO analysis of gene expression indicated that the top 20 biological processes altered in WT muscles expressing AAV-GFP-MBNL1Δ-decoy are linked to immune response similarly to AAV-GFP treated muscles (**Supplementary Fig. 9**). Pathways of muscle dysfunction were not highlighted in WT mice expressing MBNL1Δ in accordance with histologic analysis showing no muscle damages. Overall, MBNL1Δ did not induce adverse effects in muscles of WT mice.

MBNL1Δ-decoy reverses disease phenotype in DM1 mice. To determine the efficacy of MBNL1Δ *in vivo*, we used the well–established HSA^{LR} DM1 mouse model expressing 220 CTG repeats in the 3'UTR of a human skeletal actin (*ACTA1*) transgene that recapitulates characteristic DM1 features in skeletal muscles such as splicing abnormalities and myotonia. *Gastrocnemius* muscles of HSA^{LR} mice were injected for 7 weeks with AAV9-GFP-MBNL1Δ vectors (1x10^{11} vg) whereas contralateral muscles received saline vehicle (**Fig. 5A)**. Combined FISH-immunofluorescence staining performed on muscle sections showed that GFP-MBNL1Δ colocalized with almost all CUGexp-RNA foci in myonuclei of treated HSA^{LR} muscles (**Fig. 5B** and **Supplementary Fig. 10**). Next, we tested effect of MBNL1Δ on a panel of 23 DM1 misspliced events previously identified in HSA^{LR} muscles but also in MBNL1 deficient mice[8,40]. The level of correction of each misspliced event is presented in **Fig. 5C**. The composite splicing index derived from these MBNL1-dependent events indicates an overall 66% correction by MBNL1Δ treatment, which also reflects the degree of recovery of the endogenous MBNL1 activity (**Fig. 5D**). No correlation with the severity was observed (R^2: 0.05; P-value: 0.72). Consistent with correction of *Clcn1 exon 7a* missplicing that is responsible for myotonia in HSA^{LR} mice[42], the increased relaxation time measured in HSA^{LR} muscles was normalized by MBNL1Δ (**Fig. 5E-F**). Furthermore, we engineered a decoy from MBNL2 to test and extend this strategy to another RBP that has also a high binding affinity for CUGexp[28]. MBNL2Δ-decoy containing the RNA binding domain but lacking the C-terminal of MBNL2 was packaged into an AAV9 vector and injected intramuscularly in *Gastrocnemius* muscles of HSA^{LR} mice. The effect of MBNL2Δ was assessed on the panel of DM1 misspliced events that are regulated by MBNL1 (**Supplementary Fig. 11)** and the composite splicing index indicates an overall 67% correction by MBNL2Δ treatment (**Fig. 5G**). Altogether these results suggest that engineered RBPs with high CUGexp-binding affinities represent attractive decoys to displace endogenous MBNL1 from CUGexp and reverse MBNL1-dependent defects.

AAV-mediated delivery sustains a long-lasting effect of MBNL1Δ-decoy in DM1 mice. To evaluate the duration of MBNL1Δ action, HSA^{LR} mice that have undergone a single intramuscular injection of AAV-GFP-MBNL1Δ were examined one year later (**Fig. 6A)**. As observed 7 weeks post-injection, the correction of splicing misregulation of *Clcn1 exon 7a*, *Atp2a1 exon 22* and *Mbnl1 exon 5* pre-mRNAs was maintained after one year in HSA^{LR} injected muscles (**Fig. 6B**). Furthermore, normalization of myotonia that is associated with an increased muscle relaxation time in HSA^{LR} mice was also sustained over this one-year period of MBNL1Δ treatment (**Fig. 6C**). At the histological level, age-dependent myopathic changes have been described in ageing HSA^{LR} mice with an increased number of internalized nuclei in muscle fibers[15]. One-year post-injection, a significant 30% reduction of the number of fibers with internal nuclei was found in MBNL1Δ-treated muscles compared to contralateral saline-injected muscles of fifteen-months-old HSA^{LR} mice indicating that MBNL1Δ does prevent, at least to some extent, the progressive muscle pathology (**Fig. 6D-E**). Thus, a single AAV-MBNL1Δ administration is sufficient to ensure a long-lasting and efficient correction of both molecular and physiologic DM1 features in skeletal muscles.

Systemic administration of AAV-MBNL1Δ-decoy corrects muscle phenotypes in DM1 mice. To further establish the proof-of-concept of therapeutic application for this decoy gene therapy, AAV9 vectors were administrated systemically in adult HSA^{LR} mice and efficacy of MBNL1Δ treatment was assessed in skeletal

muscles (**Fig. 7A**). MBNL1Δ was fused to a small V5-tag rather than the large GFP-tag and this construct as well as MBNL1Δ without tag were validated beforehand by intramuscular AAV-injections in HSA^{LR} mice (**Extended Data Fig. 3A).** Seven weeks after systemic AAV-V5-MBNL1Δ delivery, splicing misregulations of *Clcn1 exon 7a*, *Atp2a1 exon 22* and *Mbnl1 exon 5* pre-mRNAs were corrected in *Gastrocnemius* and *Quadriceps* muscles of the same mice (**Fig. 7B and Extended Data Fig. 3B**). In accordance with correction of *Clcn1* splicing, delayed muscle relaxation time in *Gastrocnemius* muscles of treated HSA^{LR} mice was normalized (**Fig. 7C**). Next, a panel of 23 DM1-misspliced events was examined in *Gastrocnemius* muscles (**Fig. 7D**) and the composite splicing index showed an overall 50% correction of splicing defects in HSA^{LR} muscle after systemic MBNL1Δ administration (**Fig. 7E)**. The total level of endogenous MBNL1 protein in *Gastrocnemius* muscles of treated-HSA^{LR} mice remained unchanged indicating that MBNL1Δ did not act through an increase of MBNL1 level (**Fig. 7F)**. Rather the expression of MBNL1Δ that is similar to endogenous MBNL1 level (**Extended Data Fig. 3C)** was sufficient to compete for CUGexp binding and to interfere with pathogenic MBNL1:CUGexp-RNA complexes. Consequently, the released endogenous MBNL1 from CUGexp led to the recovery of MBNL1 splicing activity (**Fig. 7E**) but also to the reduction of CUGexp-transcript levels (**Fig. 7G**) as observed in MBNL1Δ-treated DM1 patient cells (**Fig. 2F**). With regard to systemic AAV administration and restricted skeletal muscle expression of CUGexp-transcripts in HSA^{LR} mice, some MBNL-dependent splicing events were assessed in other tissues that are efficiently transduced by AAV9 vectors[39]. No significant splicing changes were observed in non-diseased tissues such as heart, liver or kidney of treated HSA^{LR} mice (**Extended Data Fig. 4A-B).** Finally, we examined immunogenic response that is a major issue for gene therapies aiming to express novel transgenes. An ELISA assay to detect MBNL1Δ antibodies was performed on sera collected from MBNL1Δ-treated HSA^{LR} mice. Seven weeks after treatment, no circulating immunoglobulins against MBNL1Δ were detected compared to pre-immune sera collected from the same mice before AAV-MBNL1Δ administration (**Fig. 7H**). Thus, MBNL1Δ expression did not elicit a transgene immune response that could compromise durable MBNL1Δ action.

Discussion

In this study, we describe a novel approach to neutralize the RNA dominant mechanism triggered by expanded CUG repeats and responsible for DM1 pathogenesis. We demonstrated that engineered-RBPs with high binding affinity for CUGexp could compete for CUGexp-binding to release functional endogenous MBNL1 from RNA foci and reverse disease-associated defects in muscle cells from DM1 patient and a DM1 mouse model. To this end, we designed a decoy from MBNL1 RBP by preserving the two tandem ZnF domains that are necessary for CUGexp-binding and removing the C-terminal region. Thus, the regulatory splicing activity of MBNL1Δ is reduced compared to MBNL1 and more importantly, the residual intrinsic activity of MBNL1Δ is limited and not sufficient to compensate for splicing changes induced by dual *MBNL1* and *MBNL2* silencing in human muscle cells. In a DM1 context, MBNL1Δ competes with MBNL1 for the binding to CUGexp and promotes the dissociation of endogenous sequestered MBNL1 from CUGexp-RNA foci. MBNL1Δ modifies the dynamic of endogenous MBNL1 from a toxic unsaturated state in which MBNL1 proteins are sequestered within CUGexp foci, to a non-toxic saturated state in which the formation of MBNL1Δ:CUGexp foci promotes MBNL1 mobility and subsequently, the recovery of a pool of free and functional MBNL1 as confirmed by the correction of DM1-misspliced events. This model is in agreement with a previous study[43] showing that the dynamic of sequestration of MBNL proteins in CUGexp-RNA foci is related to the number of MBNL-binding sites on CUGexp. Interestingly, the binding of MBNL1Δ to CUGexp also leads to a reduction in the number of RNA foci per nucleus and a decrease of CUGexp-*DMPK* transcript levels. Similar effects on the stability or turn-over of CUGexp-RNAs have already been described for CAG-antisense strategies aimed at displacing MBNL1 from CUGexp[14,44,16]. Here we have provided new evidences that the C-terminal part of MBNL1 promotes intermolecular and/or intramolecular interactions leading to higher crosslinking of CUG repeats into hydrogel-like structures that facilitate CUGexp-RNA aggregation and help stabilize CUGexp-transcripts into foci. Conversely, the removal of this domain in MBNL1Δ leads to the formation of less stable CUGexp-RNA aggregates, which results in a reduced number of RNA foci confirmed by a decrease in CUGexp-transcript levels. Kinetics performed in DM1 cells demonstrated that displacement and release of free MBNL1 associated with the behavioral changes of RNA foci triggered by MBNL1Δ occur prior the progressive correction of MBNL1-dependent splicing defects supporting the mechanism of decoy action for MBNL1Δ. Nevertheless, CUGexp-RNA foci are still present in DM1 muscle cells and HSA^{LR} muscle fibers treated with MBNL1Δ despite the reversal of DM1-associated defects suggesting that nuclear CUGexp-RNA foci per se are not necessarily toxic, depending on their composition.

To further investigate the therapeutic potential of a decoy gene therapy based on engineered RBP that reverses splicing misregulations and improves the transcriptomic signature of muscle cells derived from DM1 patient, we packaged MBNL1Δ into an AAV9 vector and used the established HSA^{LR} DM1 mouse model expressing CUGexp-RNA in skeletal muscles. Our results showed that disease phenotypes of HSA^{LR} mice

were corrected following administration of AAV9-MBNL1Δ-decoy. Interfering with deleterious CUGexp:MBNL1 interaction is an approach that is currently under development with antisense oligonucleotides or small molecules aimed at targeting CUGexp repeats but requiring repeated treatments while having good penetration in muscle tissue, selectivity for CUGexp and limited off-target effects. In the proposed viral-based strategy, a single systemic administration of AAV9 vector enables an efficient delivery of MBNL1Δ-decoy in skeletal muscles but also ensures its continuous and sustained expression. In addition, RNA sequencing performed on skeletal muscles of WT mice expressing MBNL1Δ-decoy did not reveal any abnormal deregulation of transcripts containing short CUG repeats compared to AAV-GFP treated muscles. As proposed for MBNL1 itself and because they share the same RNA binding domain, the extent of MBNL1Δ binding should be proportional to the size of CUG repeats[6]. Global transcriptome analysis indicated that MBNL1Δ did not act in a dominant negative manner on MBNL1-dependent alternative splicing events or on the expression of direct MBNL1 targets. Furthermore, no histologic changes or damages were observed in muscles of WT mice expressing MBNL1Δ unlike the overexpression of MBNL1. The level of functional MBNL1 appears to be critical as MBNL1 overexpression that corrects splicing defects and myotonia in HSA^{LR} mice has deleterious effects in WT mice. Likewise and depending on the level of MBNL1 overexpression, the disease phenotype of DM1 mouse models can either be reversed or worsened[30,31]. Here, the level of endogenous MBNL1 remains unchanged in skeletal muscles of MBNL1Δ-treated WT or HSA^{LR} mice. In a DM1 context, the decoy action of MBNL1Δ will release free and functional endogenous MBNL1 from CUGexp-RNA foci, which is different from a compensatory action mediated by exogenous MBNL1 overexpression. Finally, the immune response against a novel transgene could limit both the efficacy and duration of this type of gene therapy. Such a concern has been described for another gene therapy based on an RNA-targeting dCas9 that actively eliminates CUGexp but requires transient immunosuppressive cotreatment for long term reversal of disease phenotypes in the same DM1 mouse model[22]. No immune response against engineered MBNL1Δ transgene that could compromise its expression has been detected in treated adult DM1- mice. In accordance with this result, beneficial effect was measured up to one-year after a single injection of AAV9-MBNL1Δ ensuring continuous and long-term expression of the decoy.

Although we have provided the proof of concept of an AAV-decoy gene therapy based on engineered RBPs for DM1, several steps still need to be taken before translating this approach into clinic. At present, the efficacy of the AAV-decoy was tested in the best studied HSA^{LR} mouse model for DM1 that has a restricted expression of repeat expansion transcript bearing 220 CUG to skeletal muscles. Since the size of pathologic repeats is larger in the skeletal muscles of DM1 patients and the expression of expanded-DMPK transcripts affects many other tissues including heart and brain, it will be informative to test the decoy approach into other models with larger repeats and multisystemic defects in order to assess its effectiveness and limitations. Then, preclinical development will require dose escalation, biodistribution and toxicity studies. But first, the choice of capsid and promoter for this AAV-mediated therapy must be considered depending on the target tissue(s). These issues were not investigated in this study for which AAV9 capsid was utilized to deliver the vector into muscle tissue and the decoy was driven by a ubiquitous CMV promoter that is not skeletal muscle specific. In conclusion, this work paves the way for the development of engineered RBPs with high affinity for pathogenic RNA expanded repeats to provide an AAV-mediated decoy intervention for DM1. Interestingly, competition between RBPs for expanded repeats has been proposed as a mechanism that modulates the severity of myotonic dystrophy type 2 (DM2) caused by the expression of CCUGexp-RNA[45]. Indeed, rbFOX1 may compete with MBNL1 binding to CCUGexp and partially release MBNL1 from RNA foci resulting in a milder toxicity of CCUGexp in DM2 compare to CUGexp in DM1, although repeat expansion in DM2 are larger than in DM1[46]. While the MBNL1Δ-decoy is a candidate for DM1, it could be tested in models of DM2, SCA8 and HLD-2 disorders for which sequestration of MBNL1 by either CCUGexp- or CUGexp-RNA has also been described[45,47,48]. Moreover, this approach could be extended to other non-coding repeat expansion disorders in which repeat RNA toxicity involves the titration and dysfunction of specific RBPs[49].

Methods

Materials. MBNL1Δ that contains amino acids 1 to 269 of MBNL1 was tagged with GFP and cloned in an all-in-one Tet-On lentiviral construct containing a hygromycin selection cassette[50] and lentiviral vectors were produced as previously described[44]. For *in-vivo* gene transfer, GFP- or V5-tagged MBNL1Δ, GFP-tagged MBNL2Δ containing amino acids 1 to 271 of MBNL2, GFP and GFP-tagged MBNL1 (41-kDa isoform) constructs were cloned downstream of the cytomegalovirus promotor in a pSMD2 plasmid allowing the production of AAV viral vectors[51]. Briefly, AAV9 vectors were prepared by tri-transfection in 293 cells using PEI transfection agent and the pSMD2 plasmid containing the selected construct described above, the pXX6

plasmid coding for the viral sequences essential for AAV production and the plasmid coding for serotype 9 capsid. Vector particles were purified on iodixanol gradient and concentrated on Amicon Ultra-15 100K columns (Merck-Millipore, USA). Each AAV vector was titrated as viral genomes (vg) per mL by quantitative real-time PCR as described elsewhere[52]. Plasmid pGEX-6P1-MBNL1 (40-kDa isoform) and pGEX-MBNLΔ were described previously[33] and the double tagged GST-MBNL1 containing five His-tag at the C-terminus was constructed by inverse PCR reaction with forward (5'-TAGCTCGAGCGGCCGCATCGT-3') and reverse (5'-GTGATGGTGATGGTGATGCAT CTGGGTAACATACTTGT-3') primers using plasmid pGEX-6P1-MBNL1 as template. Mini-gene expressing either cardiac Troponin T (cTNT) exon 5[53] or Insulin Receptor (INSR) exon 11[10] and DT960 plasmid (*DMPK 3'UTR* containing 960 interrupted CTG repeats, gift from Cooper T.) were used in co-transfection experiments.

Cell cultures. Human immortalized myoblasts derived from a healthy individual and a DM1 patient with 2600 CTG were grown as previously described[37]. Myoblasts were transduced with Tet-On GFP-MBNL1Δ lentiviral vectors and selected in the presence of hygromycin (1 μg/mL, Life Technologies) for one week. Induction of the conditional Tet-On GFP-MBNLΔ construct was achieved by adding doxycycline (4 µg/mL, Sigma-Aldrich) into the cell culture medium. For gene silencing experiments, differentiated muscle cells were transfected by a mix of siRNA (Eurogentec) directed against *MBNL1* and *MBNL2* mRNAs (**Table S4**) using Lipofectamine RNAiMAX reagent (Life Technologies) as described previously[54]. For mini-gene experiments, HeLa cells (ECACC 93021013) were grown to 70% confluency and co-transfected with 1μg of mini-gene plasmid, 1μg of DT960 plasmid and 3μg of GFP-MBNL1 or -MBNL1Δ plasmid using FuGENE HD transfection reagent (Roche Diagnostics, Indianapolis, USA) according to the manufacturer's instructions.

Fluorescent *in situ* hybridization (FISH) and immunofluorescence. FISH and combined FISH-Immunofluorescence experiments were performed as described previously[55] using a Cy3-labeled 2′OMe (CAG)7 probe and the following antibodies: a polyclonal anti-GFP antibody Alexa 488 conjugate (A-21311, Life Technologies, 1:200) for detection of GFP-MBNL1Δ or a polyclonal anti-MBNL1 antibody (A2764, gift from Thornton C.A, 1:1000) followed by a secondary Alexa Fluor 647-conjugated goat anti-rabbit (A-11029, Life technologies, 1:500) for detection of endogenous MBNL1. Prior fixation with 4% paraformaldehyde solution, differentiated cells grow on gelatin-coated glass coverslips were permeabilized in a CytoSkeletal buffer[56] (100 mM NaCl, 300 mM Sucrose, 10 mM PIPES, pH 6.8, 3 mM MgCl2) for 3 min at 4 °C. Pictures were captured using a Nikon Ti2 microscope equipped with a motorized stage and a CSU-W1 spinning disk head (Yokogawa) coupled with a Prime 95 sCMOS camera (Photometrics). Analyses of the number/shape of foci and intensity of MBNL1 signal were performed using Fiji software[57] and custom scripts using 3D object counter plugin[58]. Sequestered MBNL1 value was calculated by the volume of each foci multiplied by the mean endogenous MBNL1 signal intensity in the foci and by the mean number of foci per nucleus.

Purification of recombinant proteins. Recombinant protein GST-MBNL1-His isoform 40 and GST-MBNL1Δ were expressed in E. coli BL21 (DE3) by 1mM IPTG for 3 hours at 25°C. Following induction, the cell pellets were extracted with B-PER™ complete bacterial protein extraction reagent (Thermoscientific) for 15 minutes at room temperature. Proteins were purified using Glutathione Uniflow resin (BD biosciences Clontech) according to standard procedure. The double tagged recombinant MBNL1 isoform 40 was secondarily purified using a His-Nickel affinity gel (Sigma-Aldricht) according to standard procedures. In all purification steps, buffers contained 10% glycerol. Purified recombinant proteins were dialyzed against 20mM Tris-HCl pH 7.4, 0.1M KCl, 12mM dithiothreitol, 0.2mM EDTA, 10% glycerol (buffer D)[13]. Recombinant GST-MBNL1-His and GST-MBNLΔ were treated by PreScission protease (GE healthcare) to eliminate the GST tag according to standard procedure. In brief 100ug of recombinant GST-proteins was treated with 2U of PreScission protease for 16h at 4° in buffer D adjusted to 150mM NaCl. The protein was then mixed with glutathione sepharose preequilibrated with the digestion buffer for 4 hrs at 4°C. The cleaved proteins were recovered after centrifugation. Purity of proteins were analyzed by 12% polyacrylamide (37.5/1) denaturing gel electrophoresis.

RNA mobility shift assays. The RNA substrate GCUGCUGUUCGCUGCUG[35] was purchased from Eurogentec and 5'end-labelled using T4 PNK (Thermofisher Scientific) with [alpha-^{32}P] ATP. Unincorporated nucleotides were removed with a microspin TM G50 column (Sigma-Aldrich). Prior to incubation the radiolabeled RNA was denaturated in 20 mM TRIS-HCl pH 7.4, 150mM NaCl, 5 mM $MgCl_2$ for 3 min at 95°C and then chilled on ice. RNA protein complexes were formed by incubating 1 µl of recombinant MBNL proteins (0 to 4000 nM) in 10 µl of reaction mixture containing 20 mM TRIS-HCl pH 7.4, 150 mM NaCl, 5 mM $MgCl_2$, 0.1 mg/ml Escherichia coli tRNA, 0.02 % NP40, 1 mM dithiothreitol, 10 % glycerol and 9 µl of labeled RNA (5 fmol). Recombinant proteins were diluted in buffer D containing 0.5 mg/ml bovine serum albumin. The incubation was for 15 min at 30°C. 5 µl of 25 % glycerol containing 0.05 % bromophenol-blue were then

added. RNA protein-complexes were separated on a 5 % native polyacrylamide gel (39/1) containing 0.5 X Tris-borate and run at 4°C for 2 hours at 150 V. Gels were dried and autoradiographed. Competition experiments were performed under the same conditions as described above with 1500 nM of recombinant GST-MBNL1-his or MBNL1 Δ with increasing amount of recombinant (1500, 2500 and 3750 nM) MBNL1Δ or GST-MBNL1-his, respectively. Binding of protein on RNA was analyzed using PhosphorImager (Molecular Imager FX, Bio-Rad) and quantified using Quantity One (Bio-Rad). The K_d (app) was calculated by GraphPad Prism as the concentration of protein that gives 50 % of the RNA bound to the protein.

Fluorescence recovery after photobleaching (FRAP) assay. FRAP experiments were carried out on Zeiss inverted 880 confocal microscope equipped with a 63x objective, a gas mixer CO_2 supply and a temperature-controlled chamber set at 37°C. All parameters were kept constant across independent experiments and conditions. To assure a proper bleaching of the entire foci structure, the bleaching area was centered on the selected foci within the nucleus. Z-scan acquisitions were performed to cover the foci depth. Five pre-bleaching scans were obtained followed by 40 bleach pulses with 488 nm laser at 100% power. After photobleaching, image acquisitions were recorded with a time between frames of 100ms for 100 cycles until plateau is reached. FRAP series were imported into ImageJ software. Z-series were first stack using Maximum intensity Z-projection along the FRAP experiment. The area of bleaching foci was defined as a region of interest (foci ROI), a control ROI (CTL ROI) of the same cell in the nucleoplasm (unbleached GFP-region) and a background control ROI (BG ROI), define in a non-fluorescent region were used to normalize for the pixel intensities to account for photobleaching of GFP and for fluctuations in laser power during the entire acquisition series. A background control ROI (BG ROI) was also defined in a non-fluorescent region. First, foci ROI and control ROI intensity were corrected for fluorescence in the background ROI (corrected foci ROI= foci ROI – BG ROI and corrected CTL ROI= CTL ROI – BG ROI), followed by the correction of fluorescence intensity between bleached and non-bleached area (final foci ROI= corrected foci ROI/ corrected CTL ROI). Since bleaching occurs at time point=6, the fluorescent intensities of the first pre-bleaching images were used to normalize the fluorescent intensity values at all subsequent timepoints. Normalized fluorescence intensities at post-bleach timepoints were used for non-linear regression analysis using PRISM software to derives approximative half life time of recovery of the FRAP. The mobile fraction was calculated from the plateau and the first post-bleach fluorescence intensity (Y0) of the fitted curve with the following equation: $(\text{Intensity}_{plateau} - \text{Intensity}_{Y0})/(1-\text{Intensity}_{Y0})$. Obtained data were statistically tested for normality (D'Agostino and Pearson omnibus normality test, PRISM software) followed by unpaired Student t-test.

***In vitro* droplet assays.** Plasmid pSP72 containing 46 CTG repeats was obtained as described previously[54]. After linearization with restriction enzyme, plasmid CTG 46 repeats was transcribed with SP6 RNA polymerase using Megascript *in vitro* transcription kit (Ambion) according to manufacturer's instructions. Fluorescent labeled CUG was obtained by adding 0.5 mM Cy3-UTP (Cliniscience) into the transcription reaction (10% Cy3-UTP substitution). Transcribed RNAs were then treated with Turbo DNase, precipitated with ethanol, purified with Monarch® RNA Cleanup kit (NEB) and resuspended in water. The integrity of the RNA was verified using agarose gel electrophoresis. For droplet assembly, Cy3-labelled RNA (500nM) was incubated in 20μl of 20mM imidazole pH7, 100mM NaCl, 10% glycerol, 0.1mM dithiothreitol for four hours at 25°. Proteins (2.5μM) was then added. The solution was placed onto a glass-bottom chambered coverslips (Ibidi 18 well, coated with 3% BSA for 15min and washed three times with H2O) and imaged immediately (and subsequently every 30 min.) using a Nikon Ti2 microscope equipped with a motorized stage and a CSU-W1 spinning disk head (Yokogawa) coupled with a Prime 95 sCMOS camera (Photometrics) with an incubation chamber at 25°. All images were acquired from within the solution interface, and performed before droplets settled onto the bottom of the coverslip. Fiji software[57] with custom scripts was used to analyze the number, size and mobility of the droplets. Briefly, after cleaning and contrast enhancing of the picture, the droplets were detected using automatic threshold function (RenyiEntropy). Then, number and size of each object were calculated automatically. For mobility assay, the number of mobile droplets was calculated by subtracting the signal of each picture with the previous one and counting the remaining objects.

RNA isolation, RT-PCR and RT-qPCR. Total RNAs were isolated using TRI-Reagent according to the manufacturer's protocol and muscle tissue were lysed using Fastprep system and Lysing Matrix D tubes (MP biomedicals). Then, one microgram of RNA was reverse transcribed using M-MLV first-strand synthesis system (Life technologies) in a total of 20 μl. One microliter of cDNA preparation was subsequently used in a semi-quantitative PCR analysis according to standard protocol (ReddyMix, Thermo Scientific). PCR amplification was carried out for 18 cycles for GFP- or V5-MBNL1Δ detection, and 30-35 cycles for splicing of pre-mRNA within the linear range of amplification for each gene. PCR products were quantified with ImageJ

software. The ratio of exon inclusion (Psi) was quantified as a percentage of inclusion relative to total intensity of isoform signals. Composite splicing index was calculated as the mean of correction of each assessed transcript for each mouse, considering the mean WT Psi values as maximum and the mean untreated HSA^{LR} Psi values as minimal. For this analysis, PCR products were quantified using the QIAxcel Advanced system (Qiagen). To quantify the mRNA expression, real-time PCR was performed using a LC480 (Roche). Reactions were performed with SYBR Green kit (Roche) according to the manufacturer's instructions. PCR cycles were a 15 min denaturation step followed by 50 cycles with a 94 °C denaturation for 15 s, 58 °C annealing for 20 s and 72 °C extension for 20 s. Mouse Rrlp0 mRNA were used as standard. Data were analyzed with the LC480 analysis software. All primers are described in Table S4.

RNA sequencing and analysis. RNA samples were treated with RQ1 RNase-free DNase according manufacturer's protocol (Promega). For human cell samples, total stranded RNA-seq was performed at the Centre National de Génotypage. After complete RNA quality control on each sample using RNA6000 Nano LabChip analysis on Bioanalyzer (Agilent), libraries were prepared using the TruSeq Stranded Total RNA with Ribo-Zero Kit (Illumina), with an input of 1 µg. Library quality was checked by Bioanalyzer analysis, and sample libraries were pooled before sequencing to reach the expected sequencing depth. Sequencing was performed on an Illumina HiSeq2000 as paired-end 100 bp reads, using Illumina TruSeq V3 reagents. For mouse samples, total stranded RNA-seq was performed at the Platform of the Institut du Cerveau. RNA quality control of each sample was realised with Tapestation 2200 (Agilent) and libraries were prepared with the KAPA mRNA hyperprep ROCHE kit, from an input of 250ng. Sequencing was performed on an Illumina NovaSeq 6000 as paired-end 150 bp reads using flowcells SP-300. RNA-seq reads were trimmed using Cutadapt(v2.10)[59] and aligned with STAR (v2.7.5a)[60]. The reference genomes used for the alignment are hg19 and mm10 for human and mouse, respectively. Quantification of transcripts followed with HTSeq(v0.12.4)[61]. All the steps where built in a Nextflow(v20.04.1)[62] pipeline. Differentially expressed (DE) genes were then identified with the use of DESeq2(v1.30.0)[63] in R-Studio environment (R v4.0.2). A cut-off of |log2-fold-change|>1 & p.adjusted <0.05 was applied to select the significantly DE genes. Differential alternative splicing was detected by rMATS(v4.1)[64], based on the STAR-aligned files (.bam). Detection of events was done with a 'prep' step of each pair of conditions (WT-vs-DM1 & WT-vs-MBNL1Δ for human, Saline-vs-MBNL1Δ & Saline-vs-GFP for mouse), a 'post' step of all conditions together and finally a 'stats' step of each pair of conditions to define *p-adjusted-value* and *InclLevelDifference* for each comparison. Finally, the correction percentage of splicing was calculated for each splicing event, based on the following formula: $(PSI_{MBNL1\Delta} - PSI_{DM1}) * 100 / (PSI_{CTRL} - PSI_{DM1})$, where PSI is the mean PSI (or "IncLevelDifference") of all replicates of a given condition, for a splicing event, as provided by rMATS results. GO terms and biological pathways enrichment analysis was done using the ToppGene suite[65].

Northern blot. Total RNA was extracted from DM1 cells using a guanidine thiocyanate solution (4 M guanidine thiocyanate, 20 mM sodium acetate pH 5.2, 0.5 % N-lauryl sarcosine and 1 % v/v b-mercaptoethanol). The lysate was loaded onto a cesium chloride cushion (5.7 M cesium chloride, 10 mM EDTA, 20 mM sodium acetate) and ultracentrifuged for 18-20 hours at 155 000 g. The pellet was resuspended in 400 µl TES solution (10 mM Tris-HCl pH 7.5, 5 mM EDTA, 0.1 % SDS) and RNA was extracted twice by acid phenol/CHCl3 (1:1) and then by CHCl3. RNA was precipitated by 0.3 M sodium acetate pH 5.2 and ethanol, washed twice with 75 % ethanol and resuspended in water. 10 µg of RNA was separated on 1.0 % agarose MESA (Sigma-Aldrich) gels containing 6 M formaldehyde and transferred onto Hybond-N+ membrane (GE Healthcare) by capillary transfer with 20xSSC. Blots were hybridized with a 32P-end-labeled (CAG)7 probe in a ULTRAhyb-Oligo hybridization buffer (Ambion-ThermoFischer) at 42°C overnight. Signals were analyzed on a phosphoimager (Molecular Imager FX, Bio-Rad) and quantified using ImageJ. All values were normalized to 18S rRNA signal after hybridization with a 32P-end-labeled 18S oligonucleotide probe.

***In vivo* gene transfer, muscle histology and muscle force.** All mouse procedures were done according to the protocol 01204.02 approved by the Ethical Committee on Animal Resources at the Centre Experimentation Fonctionnelle of Pitié-Salpétrière animal facility and under appropriate biological containment. Briefly, mice were maintained in a conventional specific-pathogen–free facility with a fixed light cycle (22°C, 12-hour dark-light cycle). Homozygous HSA^{LR} (Long Repeat, line 20b) transgenic mice (kindly provided by C. Thornton) were used in this study and genotyped for HSA^{LR} transgenes by quantification of *ACTA1* levels normalized to endogenous mouse *Acta1* in genomic DNA. Mice of the corresponding background strain (FVB/N) were used as control. Three months-old adult control FVB or HSA^{LR} mice were injected with saline or AAV9 vectors either intramuscularly (*Gastrocnemius*) or systemically (retro-orbital sinus). At sacrifice, heart, liver and kidney were snap-frozen in liquid nitrogen and muscles were snap-frozen

in isopentane chilled with liquid nitrogen. Muscles were then sliced at 10 µm with a cryostat and hematoxylin and eosin (H&E) staining was done according to the standard procedures. Images were captured by Leica DMR microscope using a NikonDS-Ri1 camera and NIS-Element software. To determine the percentage of muscle fibers with internal nuclei, more than 1200 fibers (5-6 fields per muscle section) were counted. The isometric contractile properties of *gastrocnemius* muscle were studied *in situ* as previously described[66]. Mice were anesthetized with a solution of Ketamine/Xylasine (80 mg.kg-1 and 15 mg.kg-1, respectively). The knee and foot were fixed with clamps and pins. The distal tendon of the GA muscle was attached to a lever arm of a servomoteur system (305B, Dual-Mode Lever). Data were recorded and analyzed using PowerLab system (4SP, ADInstruments) and software (Chart 4, ADInstruments). The sciatic nerve (proximally crushed) was stimulated by a bipolar silver electrode using a supramaximal (10-V) square wave pulse of 0.1 ms duration. Absolute maximal isometric tetanic force (P0) was measured during isometric contractions in response to electrical stimulation (frequency of 25 to 150 Hz, train of stimulation of 500 ms). Myotonia is measured as the increase in the area under the relaxation force/time curve.

Western-Blot. Tissue samples were lysed in RIPA buffer (150 mM NaCl, 50 mM Tris-HCl pH 8, 0.1 mM ethylenediamine tetra-acetic acid (EDTA), 1% NP-40, 0.5% sodium dodecyl sulfate (SDS) supplemented with Complete Protease Inhibitor Cocktail (Roche). Lysates were sonicated and centrifuged at 14 000 g for 10 min at 4°C. Protein concentration was determined by BCA assay (Thermo scientific). Samples were diluted in Laemmli Reducing Sample Buffer supplemented with 50mM DTT, heated to 70°C for 5 min, separated on 4-12% Bis-Tris polyacrylamide gels (Thermo scientific) and transferred to nitrocellulose membrane (Porablot NCP, Macherey-Nagel) using a wet transfer apparatus (1 h, 100 V, 4°C). Membranes were blocked for 1 h in 5% milk in PBST buffer (phosphate buffered saline, 0.1% Tween-20) and incubated with a primary antibody against MBNL1 (A2764, 1:1000 or MB1a, gift from Holt I. and Morris G., 1:1000), V5 (Life Technologies, 1:1000) GFP (Clontech, 1:1000), GAPDH (Santa Cruz, 1:1000) or VINCULIN (Sigma, 1:1000,). Anti-rabbit (Life Technologies, 1:20 000) and anti-mouse (Invitrogen, 1:20000) secondary antibodies were conjugated with horseradish peroxidase and detected using the Immobilon Western Chemiluminescent HRP Substrate system (EMD Millipore).

ELISA assay. Blood samples from individual mice were collected twice (one day before systemic injection of saline or AAV-MBNL1Δ vectors and seven weeks post-injection, one day before sacrifice) and serum was separated from blood within 1 h by centrifugation. Maxisorp plates (Nunc, France) were coated with 100 µL per well of purified MBNL1Δ proteins or unrelated AKAP4-GFP proteins diluted at 1 mg/mL in carbonate buffer pH 9.6. The coating solution was incubated overnight at 4°C and replaced by a PBS buffer containing casein (0.1%) for 30 minutes at 37°C that. After three washes with PBS/Tween-20 (0.05%), serum or MB1a antibody diluted in a PBS/BSA (0.2%) buffer were added for two hours at room temperature. MB1a monoclonal antibody is directed against an epitope located in the linker encodes by MBNL1 exon 3 and presents in MBNL1Δ). After three washes, secondary antibody diluted in PBS/BSA (0.2%) was added for 1 hour and then, five additional washes were performed. Finally, 100 µL of soluble One-component TMB Substrate (ThermoFisher scientific) was added to each well and the reaction was stopped by adding 50μL of sulfonic acid. Absorbance of each well was measured at 450nm.

Statistical analysis. All statistical analyses were performed using the GraphPad Prism software (Version 6, GraphPad Software Inc.). Data distribution was assessed by the Kolmogorov-Smirnov test prior to the use of either Student *t*-test or one-way ANOVA analyses of variance as appropriate.

Reporting Summary. Further information on research design is available in the Nature Research Reporting Summary linked to this article

Data availability

The main data supporting the results in this study are available within the paper and its Supplementary Information. NGS data are available at the GEO repository (GSE189516). The raw and analyzed datasets generated during the study are available for research purposes from the corresponding author on reasonable request.

References

1. Lukong, K. E., Chang, K., Khandjian, E. W. & Richard, S. RNA-binding proteins in human genetic disease. *Trends Genet. TIG* **24**, 416–425 (2008).

2. Lin, X. *et al.* Failure of MBNL1-dependent post-natal splicing transitions in myotonic dystrophy. *Hum. Mol. Genet.* **15**, 2087–2097 (2006).
3. Kanadia, R. N. *et al.* A muscleblind knockout model for myotonic dystrophy. *Science* **302**, 1978–1980 (2003).
4. Brook, J. D. *et al.* Molecular basis of myotonic dystrophy: expansion of a trinucleotide (CTG) repeat at the 3' end of a transcript encoding a protein kinase family member. *Cell* **69**, 385 (1992).
5. Taneja, K. L., McCurrach, M., Schalling, M., Housman, D. & Singer, R. H. Foci of trinucleotide repeat transcripts in nuclei of myotonic dystrophy cells and tissues. *J. Cell Biol.* **128**, 995–1002 (1995).
6. Miller, J. W. *et al.* Recruitment of human muscleblind proteins to (CUG)(n) expansions associated with myotonic dystrophy. *EMBO J.* **19**, 4439–4448 (2000).
7. Lee, K.-Y. *et al.* Compound loss of muscleblind-like function in myotonic dystrophy. *EMBO Mol. Med.* **5**, 1887–1900 (2013).
8. Nakamori, M. *et al.* Splicing biomarkers of disease severity in myotonic dystrophy. *Ann. Neurol.* **74**, 862–872 (2013).
9. Mankodi, A. *et al.* Expanded CUG repeats trigger aberrant splicing of ClC-1 chloride channel pre-mRNA and hyperexcitability of skeletal muscle in myotonic dystrophy. *Mol. Cell* **10**, 35–44 (2002).
10. Savkur, R. S., Philips, A. V. & Cooper, T. A. Aberrant regulation of insulin receptor alternative splicing is associated with insulin resistance in myotonic dystrophy. *Nat. Genet.* **29**, 40–47 (2001).
11. Fugier, C. *et al.* Misregulated alternative splicing of BIN1 is associated with T tubule alterations and muscle weakness in myotonic dystrophy. *Nat. Med.* **17**, 720–725 (2011).
12. Rau, F. *et al.* Abnormal splicing switch of DMD's penultimate exon compromises muscle fibre maintenance in myotonic dystrophy. *Nat. Commun.* **6**, 7205 (2015).
13. Freyermuth, F. *et al.* Splicing misregulation of SCN5A contributes to cardiac-conduction delay and heart arrhythmia in myotonic dystrophy. *Nat. Commun.* **7**, 11067 (2016).
14. Wheeler, T. M. *et al.* Reversal of RNA dominance by displacement of protein sequestered on triplet repeat RNA. *Science* **325**, 336–339 (2009).
15. Wheeler, T. M. *et al.* Targeting nuclear RNA for in vivo correction of myotonic dystrophy. *Nature* **488**, 111–115 (2012).
16. Klein, A. F. *et al.* Peptide-conjugated oligonucleotides evoke long-lasting myotonic dystrophy correction in patient-derived cells and mice. *J. Clin. Invest.* **129**, 4739–4744 (2019).
17. Warf, M. B., Nakamori, M., Matthys, C. M., Thornton, C. A. & Berglund, J. A. Pentamidine reverses the splicing defects associated with myotonic dystrophy. *Proc. Natl. Acad. Sci. U. S. A.* **106**, 18551–18556 (2009).
18. García-López, A., Llamusí, B., Orzáez, M., Pérez-Payá, E. & Artero, R. D. In vivo discovery of a peptide that prevents CUG-RNA hairpin formation and reverses RNA toxicity in myotonic dystrophy models. *Proc. Natl. Acad. Sci. U. S. A.* **108**, 11866–11871 (2011).
19. Angelbello, A. J. *et al.* Precise small-molecule cleavage of an r(CUG) repeat expansion in a myotonic dystrophy mouse model. *Proc. Natl. Acad. Sci. U. S. A.* **116**, 7799–7804 (2019).
20. Nakamori, M., Taylor, K., Mochizuki, H., Sobczak, K. & Takahashi, M. P. Oral administration of erythromycin decreases RNA toxicity in myotonic dystrophy. *Ann. Clin. Transl. Neurol.* **3**, 42–54 (2016).
21. Batra, R. *et al.* Elimination of Toxic Microsatellite Repeat Expansion RNA by RNA-Targeting Cas9. *Cell* **170**, 899-912.e10 (2017).
22. Batra, R. *et al.* The sustained expression of Cas9 targeting toxic RNAs reverses disease phenotypes in mouse models of myotonic dystrophy type 1. *Nat. Biomed. Eng.* **5**, 157–168 (2021).
23. Zhang, N., Bewick, B., Xia, G., Furling, D. & Ashizawa, T. A CRISPR-Cas13a Based Strategy That Tracks and Degrades Toxic RNA in Myotonic Dystrophy Type 1. *Front. Genet.* **11**, 594576 (2020).
24. Kanadia, R. N. *et al.* Reversal of RNA missplicing and myotonia after muscleblind overexpression in a mouse poly(CUG) model for myotonic dystrophy. *Proc. Natl. Acad. Sci. U. S. A.* **103**, 11748–11753 (2006).
25. Hale, M. A. *et al.* An engineered RNA binding protein with improved splicing regulation. *Nucleic Acids Res.* **46**, 3152–3168 (2018).
26. Konieczny, P., Stepniak-Konieczna, E. & Sobczak, K. MBNL proteins and their target RNAs, interaction and splicing regulation. *Nucleic Acids Res.* **42**, 10873–10887 (2014).
27. Kanadia, R. N. *et al.* Developmental expression of mouse muscleblind genes Mbnl1, Mbnl2 and Mbnl3. *Gene Expr. Patterns GEP* **3**, 459–462 (2003).
28. Fardaei, M. *et al.* Three proteins, MBNL, MBLL and MBXL, co-localize in vivo with nuclear foci of expanded-repeat transcripts in DM1 and DM2 cells. *Hum. Mol. Genet.* **11**, 805–814 (2002).
29. Chen, G. *et al.* Altered levels of the splicing factor muscleblind modifies cerebral cortical function in mouse models of myotonic dystrophy. *Neurobiol. Dis.* **112**, 35–48 (2018).

30. Chamberlain, C. M. & Ranum, L. P. W. Mouse model of muscleblind-like 1 overexpression: skeletal muscle effects and therapeutic promise. *Hum. Mol. Genet.* **21**, 4645–4654 (2012).
31. Yadava, R. S. *et al.* MBNL1 overexpression is not sufficient to rescue the phenotypes in a mouse model of RNA toxicity. *Hum. Mol. Genet.* **28**, 2330–2338 (2019).
32. Shukla, T. N., Song, J. & Campbell, Z. T. Molecular entrapment by RNA: an emerging tool for disrupting protein-RNA interactions in vivo. *RNA Biol.* **17**, 417–424 (2020).
33. Tran, H. *et al.* Analysis of exonic regions involved in nuclear localization, splicing activity, and dimerization of Muscleblind-like-1 isoforms. *J. Biol. Chem.* **286**, 16435–16446 (2011).
34. Grammatikakis, I., Goo, Y.-H., Echeverria, G. V. & Cooper, T. A. Identification of MBNL1 and MBNL3 domains required for splicing activation and repression. *Nucleic Acids Res.* **39**, 2769–2780 (2011).
35. Warf, M. B. & Berglund, J. A. MBNL binds similar RNA structures in the CUG repeats of myotonic dystrophy and its pre-mRNA substrate cardiac troponin T. *RNA N. Y. N* **13**, 2238–2251 (2007).
36. Wagner, S. D. *et al.* Dose-Dependent Regulation of Alternative Splicing by MBNL Proteins Reveals Biomarkers for Myotonic Dystrophy. *PLoS Genet.* **12**, e1006316 (2016).
37. Arandel, L. *et al.* Immortalized human myotonic dystrophy muscle cell lines to assess therapeutic compounds. *Dis. Model. Mech.* **10**, 487–497 (2017).
38. Jain, A. & Vale, R. D. RNA phase transitions in repeat expansion disorders. *Nature* **546**, 243–247 (2017).
39. Zincarelli, C., Soltys, S., Rengo, G. & Rabinowitz, J. E. Analysis of AAV Serotypes 1–9 Mediated Gene Expression and Tropism in Mice After Systemic Injection. *Mol. Ther.* **16**, 1073–1080 (2008).
40. Tanner, M. K., Tang, Z. & Thornton, C. A. Targeted splice sequencing reveals RNA toxicity and therapeutic response in myotonic dystrophy. *Nucleic Acids Res.* **49**, 2240–2254 (2021).
41. Wang, E. T. *et al.* Transcriptome-wide regulation of pre-mRNA splicing and mRNA localization by muscleblind proteins. *Cell* **150**, 710–724 (2012).
42. Wheeler, T. M., Lueck, J. D., Swanson, M. S., Dirksen, R. T. & Thornton, C. A. Correction of ClC-1 splicing eliminates chloride channelopathy and myotonia in mouse models of myotonic dystrophy. *J. Clin. Invest.* **117**, 3952–3957 (2007).
43. Sznajder, Ł. J. *et al.* Mechanistic determinants of MBNL activity. *Nucleic Acids Res.* **44**, 10326–10342 (2016).
44. François, V. *et al.* Selective silencing of mutated mRNAs in DM1 by using modified hU7-snRNAs. *Nat. Struct. Mol. Biol.* **18**, 85–87 (2011).
45. Liquori, C. L. *et al.* Myotonic dystrophy type 2 caused by a CCTG expansion in intron 1 of ZNF9. *Science* **293**, 864–867 (2001).
46. Sellier, C. *et al.* rbFOX1/MBNL1 competition for CCUG RNA repeats binding contributes to myotonic dystrophy type 1/type 2 differences. *Nat. Commun.* **9**, 2009 (2018).
47. Daughters, R. S. *et al.* RNA Gain-of-Function in Spinocerebellar Ataxia Type 8. *PLoS Genet.* **5**, e1000600 (2009).
48. Rudnicki, D. D. *et al.* Huntington's disease--like 2 is associated with CUG repeat-containing RNA foci. *Ann. Neurol.* **61**, 272–282 (2007).
49. Swinnen, B., Robberecht, W. & Van Den Bosch, L. RNA toxicity in non-coding repeat expansion disorders. *EMBO J.* **39**, e101112 (2020).
50. Chaouch, S. *et al.* Immortalized skin fibroblasts expressing conditional MyoD as a renewable and reliable source of converted human muscle cells to assess therapeutic strategies for muscular dystrophies: validation of an exon-skipping approach to restore dystrophin in Duchenne muscular dystrophy cells. *Hum. Gene Ther.* **20**, 784–790 (2009).
51. Snyder, R. O. *et al.* Efficient and stable adeno-associated virus-mediated transduction in the skeletal muscle of adult immunocompetent mice. *Hum. Gene Ther.* **8**, 1891–1900 (1997).
52. Moulay, G. *et al.* Alternative splicing of clathrin heavy chain contributes to the switch from coated pits to plaques. *J. Cell Biol.* **219**, e201912061 (2020).
53. Cooper, T. A. Muscle-specific splicing of a heterologous exon mediated by a single muscle-specific splicing enhancer from the cardiac troponin T gene. *Mol. Cell. Biol.* **18**, 4519–4525 (1998).
54. Laurent, F.-X. *et al.* New function for the RNA helicase p68/DDX5 as a modifier of MBNL1 activity on expanded CUG repeats. *Nucleic Acids Res.* **40**, 3159–3171 (2012).
55. Klein, A. F., Arandel, L., Marie, J. & Furling, D. FISH Protocol for Myotonic Dystrophy Type 1 Cells. *Methods Mol. Biol. Clifton NJ* **2056**, 203–215 (2020).
56. Byron, M., Hall, L. L. & Lawrence, J. B. A multifaceted FISH approach to study endogenous RNAs and DNAs in native nuclear and cell structures. *Curr. Protoc. Hum. Genet.* **Chapter 4**, Unit 4.15 (2013).
57. Schindelin, J. *et al.* Fiji: an open-source platform for biological-image analysis. *Nat. Methods* **9**, 676–682 (2012).

58. Bolte, S. & Cordelières, F. P. A guided tour into subcellular colocalization analysis in light microscopy. *J. Microsc.* **224**, 213–232 (2006).
59. Martin, M. Cutadapt removes adapter sequences from high-throughput sequencing reads. *EMBnet.journal* **17**, 10–12 (2011).
60. Dobin, A. *et al.* STAR: ultrafast universal RNA-seq aligner. *Bioinformatics* **29**, 15–21 (2013).
61. Anders, S., Pyl, P. T. & Huber, W. HTSeq—a Python framework to work with high-throughput sequencing data. *Bioinformatics* **31**, 166–169 (2015).
62. Nextflow enables reproducible computational workflows - PubMed. https://pubmed.ncbi.nlm.nih.gov/28398311/.
63. Love, M. I., Huber, W. & Anders, S. Moderated estimation of fold change and dispersion for RNA-seq data with DESeq2. *Genome Biol.* **15**, 550 (2014).
64. Shen, S. *et al.* rMATS: Robust and flexible detection of differential alternative splicing from replicate RNA-Seq data. *Proc. Natl. Acad. Sci. U. S. A.* **111**, E5593–E5601 (2014).
65. Chen, J., Bardes, E. E., Aronow, B. J. & Jegga, A. G. ToppGene Suite for gene list enrichment analysis and candidate gene prioritization. *Nucleic Acids Res.* **37**, W305-311 (2009).
66. Hourdé, C. *et al.* Sustained peripheral arterial insufficiency durably impairs normal and regenerating skeletal muscle function. *J. Physiol. Sci. JPS* **56**, 361–367 (2006).

Acknowledgements
This work was supported by grants from ANR (Agence National de la Recherche), AFM (Association Francaise contre les Myopathies) and Association Institut de Myologie. M.M was supported by the DIM biotherapies, Paris Ile-de-France Region. We thank I. Holt and G. Morris (CIND, RJAH Orthopeadic Hospital, UK) as well as “The Muscular Dystrophy Association Monoclonal Antibody Resource” for the MBNL1 (MB1a) antibody, T. Cooper for the 960 CTG construct, C. Thornton for the MBNL1 polyclonal antibody and the HSA^{LR} mouse model, the iVector facility of the Institut du Cerveau, the human cell immortalization facility as well as the AAV facility of the Myology Institute, the Penn Vector Core -Gene Therapy Program- University of Pennsylvania (Philadelphia) for providing the pAAV2/9 plasmid (p5E18-VD29). We also thank Cadot B., Ziyyat-Benkhelifa S., Julien L., Jollet A., Neuillet C. and Allamand V. for their help.

Author contributions
L.A. and M.M. conducted most of the experiments. F.R. performed FRAP experiments, J.M and A.K. performed LLPS experiments, and M.N., A.K., A.S., J.M., A.C., T.H., C.L. and L.B. supported some experiments. C.M. and B.S. produced lentiviral vectors, A.F. and M.L. measured the muscle force, and M.P-E., M.K. and N.N. performed RNAseq analysis. N.S. and D.F. supervised the project and wrote the manuscript.

Competing interests
The method described in this paper is the subject of a patent application. The authors declare no other competing financial interest.

Additional information [please do not modify this section]
Supplementary information The online version contains supplementary material available at https://doi.org/10.1038/s41551-01X-XXXX-X.
Correspondence and requests for materials should be addressed to Denis Furling
Peer review information *Nature Biomedical Engineering* thanks Reviewer and the other, anonymous, reviewer(s) for their contribution to the peer review of this work. Peer reviewer reports are available.
Reprints and permissions information is available at www.nature.com/reprints.
Publisher’s note: Springer Nature remains neutral with regard to jurisdictional claims in published maps and institutional affiliations.

Figures

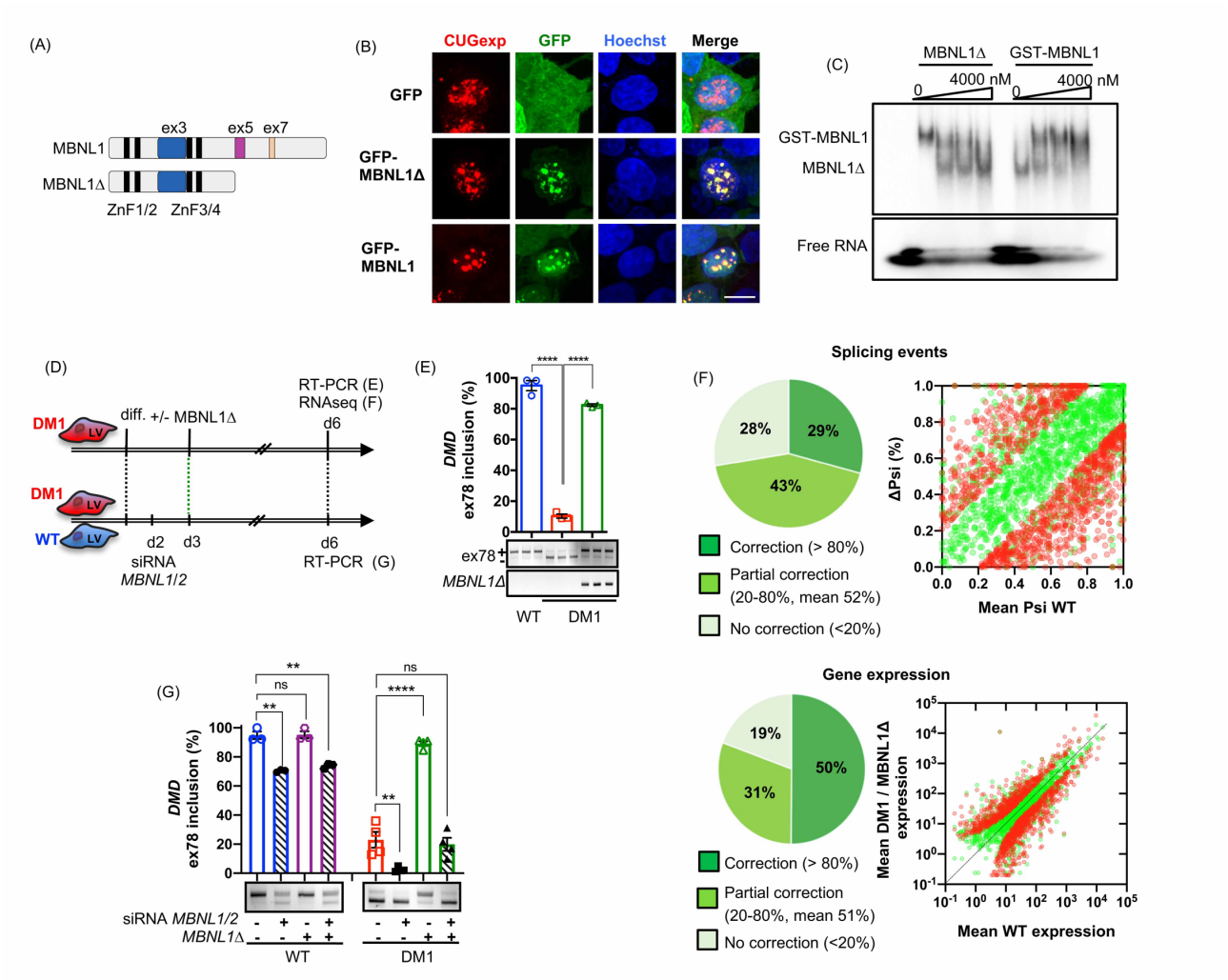

Fig. 1 | MBNL1Δ corrects alternative splicing defects and overall transcriptome of DM1 patient-derived muscle cells. A, Schematic representation of MBNL1 and MBNL1Δ proteins: zinc finger domains and alternative exon 3, 5 and 7 are indicated by black, blue, pink and orange boxes, respectively. **B**, CUGexp-RNA foci and MBNL1 or MBNL1Δ visualized by combined RNA-FISH/immunofluorescence in Hela cells co-transfected with plasmids expressing 960 CTG repeats and GFP-MBNL1 or GFP-MBNL1Δ. CUGexp-RNA foci detected with a Cy3-CAG probe (red), GFP-MBNL proteins using an anti-GFP antibody (green) and nuclei by Hoechst staining (blue). **C**, Competition between GST-MBNL1 and MBNL1Δ for binding to p32 labelled CUGexp-RNA determined by electrophoresis mobility shift assay. **(D)** Experimental design: immortalized DM1 myoblasts transduced with conditional GFP-MBNL1Δ lentiviral vectors (LV) and differentiated for 3 days before the addition of Dox allowing GFP-MBNL1Δ expression and further analysis (E-F) at day 6. In a comparable experimental set up, siRNA against *MBNL1* and *MBNL2* were transfected at day 2/3 of differentiation in both WT and DM1 muscle cells (G). **E**, Correction of misregulation of *DMD exon 78* alternative splicing assessed by RT-PCR in differentiated DM1 muscle cells expressing GFP-MBNL1Δ (n=3). Data analyzed by one-way ANOVA followed by Tukey's test (****$p< 0.0001$). **F**, Pie charts of transcriptomic analyses showed overall correction of splicing defects (upper panel) and gene expression deregulation (lower panel) in GFP-MBNL1Δ-expressing DM1 muscles cells (n=3) compared to WT (n=6) and non-treated DM1 muscle cells (n=3). Corresponding plot charts showed the distribution of DM1 events before (in red) and after (in green) MBNL1Δ treatment. **G**, Correction of misregulations of *DMD exon 78* alternative splicing in differentiated WT and DM1 muscle cells expressing or not GFP-MBNL1Δ and transfected with or without siRNA against *MBNL1* and *MBNL2* mRNAs (n=4). Data analyzed by one-way ANOVA followed by Tukey's test (***$p < 0.001$, ****$p < 0.0001$, ns: no significant).

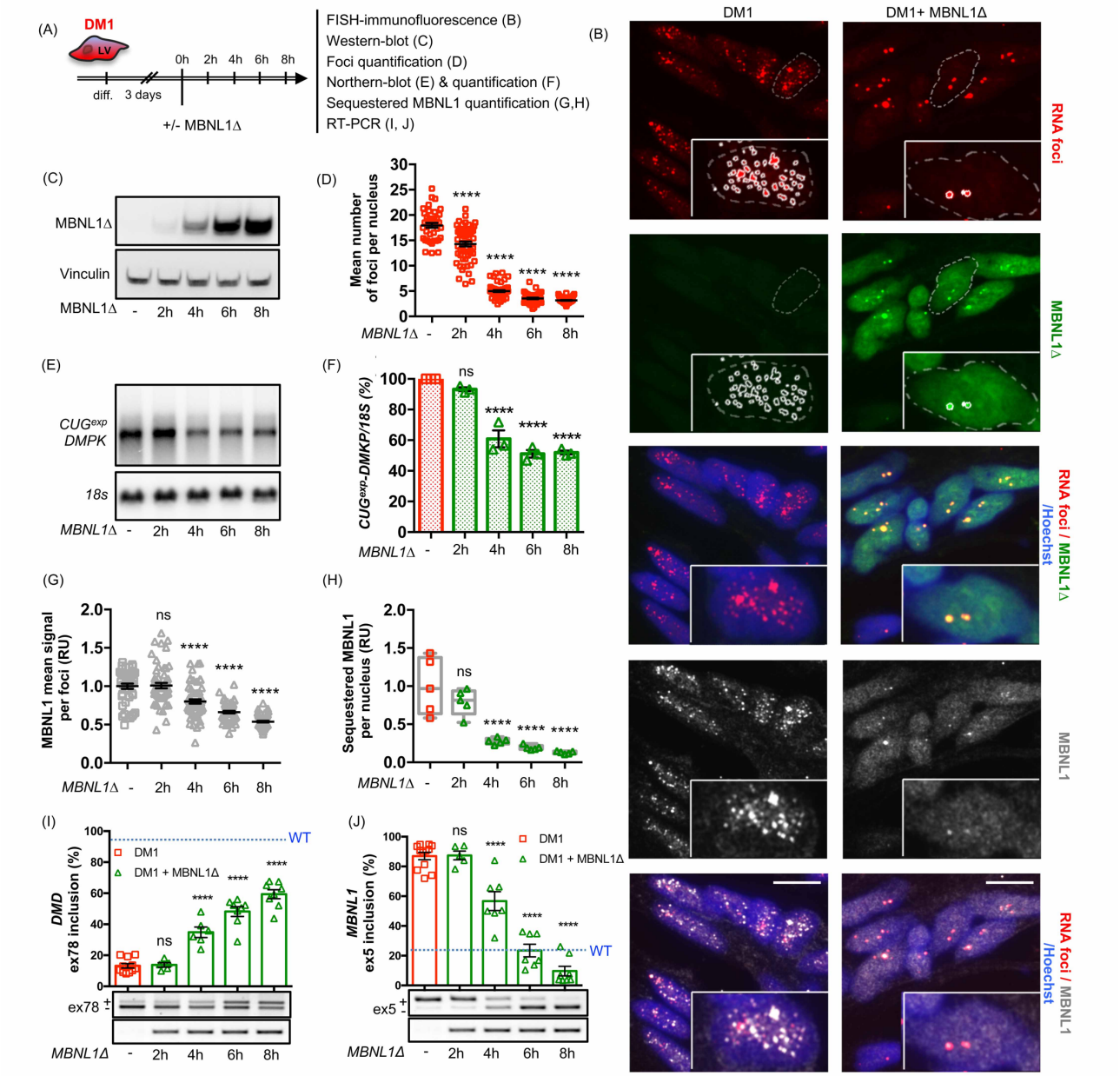

Fig. 2 | MBNL1Δ binding to CUGexp displaces endogenous MBNL1 from RNA foci and reduces CUGexp-RNA levels in DM1 patient-derived muscle cells. A, Experimental design: induction of GFP-MBNL1Δ in differentiated DM1 muscle cells and immediate consequences. **B**, CUGexp-RNA foci, MBNL1Δ and MBNL1 visualized by combined RNA FISH/ immunofluorescence in differentiated DM1 muscle cells expressing or not GFP-MBNL1Δ for 8h. Representative images of time points 0 and 8h were duplicated from Supplementary Fig. 4 showing all time points (0, 2, 4, 6, 8h). CUGexp-RNA foci detected with a Cy3-CAG probe (red), GFP-MBNL1Δ using an anti-GFP antibody (green), endogenous MBNL1 with a polyclonal antibody directed against the C-ter part of the protein (grey) and nuclei with Hoechst staining (blue). Nucleus perimeter represented by dotted line in upper panels and ROI identified for foci analysis indicated by solid white lines. Scale bar: 10μm. **C**, GFP-MBNLΔ expression in DM1 muscle cells after Dox-induction. **(D)** Quantification of the mean number of foci per nucleus in DM1 muscle cells following MBNL1Δ expression. Data analyzed by one-way ANOVA followed by Tukey's test (****p<0.0001). **E-F**, Levels of *CUGexp-DMPK* transcripts determined by Northern Blot in differentiated DM1 muscles cells following MBNL1Δ expression (n=3). Data were analyzed by one-way ANOVA followed by Tukey's test (****$p < 0.0001$, ns=no significant). **G-H**, MBNL1 mean signal per foci (G) and mean sequestered MBNL1 level per nucleus (H, mean volume*intensity*number of foci) quantified in DM1 muscle cells expressing or not MBNL1Δ (n>50 fields from 5 experiments and more than 45 nuclei per n). Data analyzed by one-way ANOVA followed by Tukey's test (****$p < 0.0001$, ns: no significant). **I-J**, Correction of *DMD exon 78* (I) and *MBNL1 exon 5* (J) alternative splicing assessed by RT-PCR in differentiated DM1 muscle cells following MBNL1Δ expression (n≥5). Data analyzed by one-way ANOVA followed by Tukey's test (****$p < 0.0001$, ns: no significant).

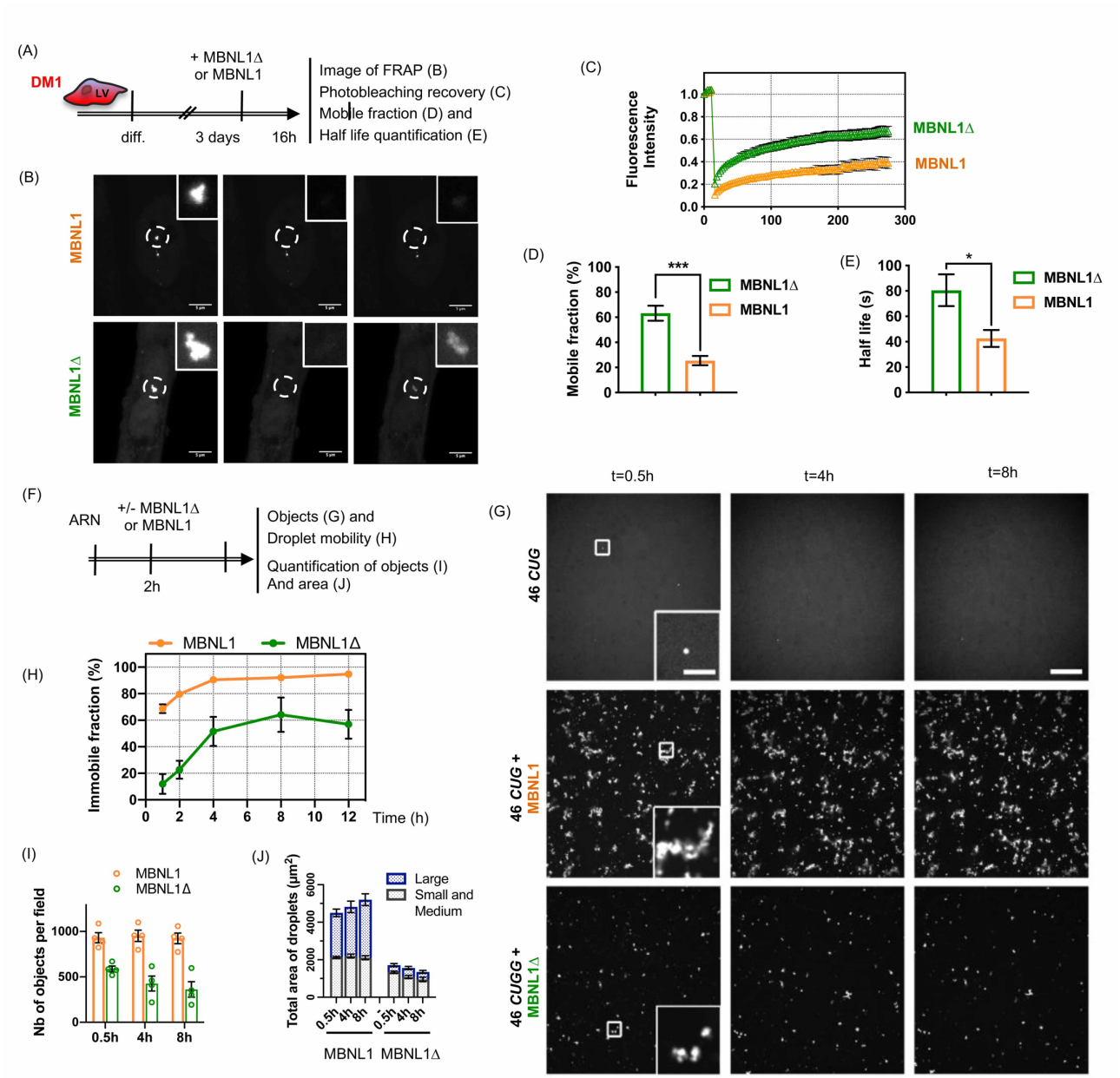

Fig. 3 | MBNL1Δ forms less stable CUGexp-RNA complexes than MBNL1. A, Fluorescence recovery after photobleaching (FRAP) experiments on DM1 cell lines expressing GFP-MBNL1 or GFP-MBNL1Δ. **B**, Representative images of FRAP experiment show z-stack from pre-bleach, bleach and plateau post-bleach time points in cells expressing GFP-MBNL1Δ or GFP-MBNL1. **C**, Recovery curves of photobleached foci are represented as normalized fluorescent intensity over time. Each data points correspond to the average of at least 25 foci, error bars indicate the sem. **D-E**, Quantification of mobile fractions and half life time of recovery obtained by non-linear regression analysis. Mean with SEM for at least n=25 foci. Significance. were tested with unpaired Student t-test (*$p < 0.05$; **$p < 0.01$; ***$p < 0.001$). **F**, Experimental schematic of *in vitro* RNA droplet assay in the presence MBNL1 or MBNL1Δ recombinant proteins. **G**, Representative images of fluorescent Cy3 RNA droplet formation in the presence of MBNL1 or MBNL1Δ recombinant proteins at different time points. 2.5 mM of MBNL1 or MBNL1Δ were added to 500nM cy3-*CUG* 46 in droplet formation buffer containing 100nM NaCl. Magnification 40x ; Scale bar 50μm ; Scale bar in insert 10μm. **H**, Percentage of immobile fraction (%) of RNA droplets at different time points after the addition of MBNL1 or MBNL1Δ recombinant proteins. **I**, Quantification of the number of fluorescent RNA droplets in the presence of MBNL1 or MBNL1Δ recombinant proteins. J) Quantification of the area occupied by the RNA droplets in the presence of MBNL1 or MBNL1Δ recombinant proteins.

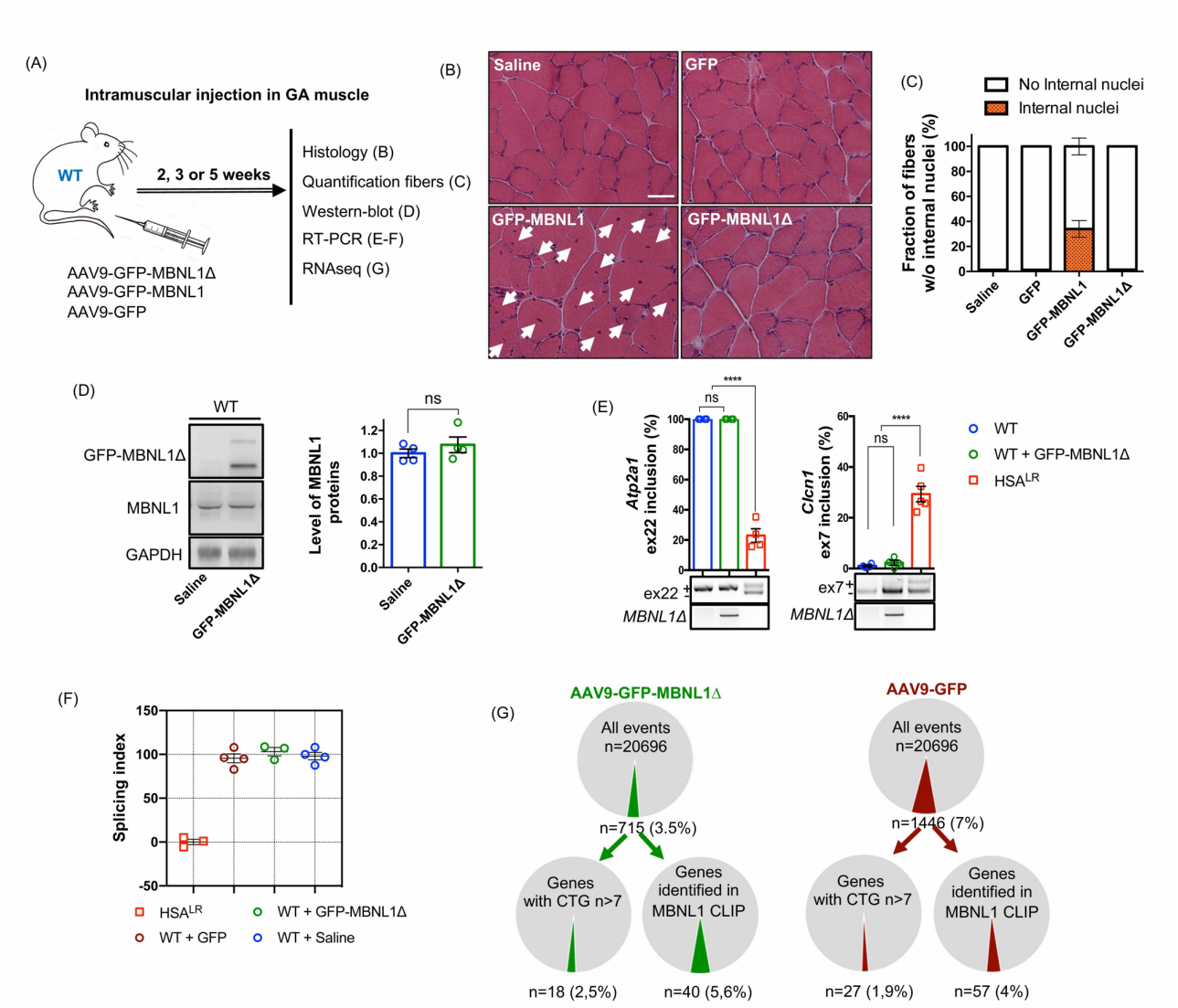

Fig. 4 | Intramuscular expression of MBNL1Δ using AAV vectors has no deleterious effect in WT mice. A, Experimental design: *Gastrocnemius* (GA) muscles of FVB mice injected with either AAV9-GFP-MBNL1Δ, AAV9-GFP-MBNL1 or AAV9-GFP vectors ($1x10^{11}$ vg, n=4) for 5 weeks. Contralateral muscles received saline vehicle. **B**, Hematoxylin and Eosin (HE) staining performed on *Gastrocnemius* cryosections. Internalized nuclei within fibers were indicated by white arrows. **C**, Fraction of fibers with or without (w/o) internal nuclei following a single intramuscular injection (n=1500 fibers per muscle). **D**, Levels of MBNL1 in muscle of WT mice injected with AAV9-GFP-MBNLΔ or saline determined by Western blot (n=4). Data analyzed by unpaired Student's t-test (ns=no significant). **E**, Splicing profiles of *Clcn1 exon 7a and Atp2a1 exon 22* assessed by RT-PCR in WT mice five weeks after intramuscular injection of AAV9-GFP-MBNL1Δ compared to saline vehicle-injected contralateral muscles or muscles form HSA^{LR} mice (n=3). Data analyzed by one-way ANOVA followed by Tukey's test (****$p < 0.0001$). **F**, Composite splicing index derived from a panel of 23 DM1-misspliced events regulated by MBNL1 and analyzed in muscle of WT mice injected with AAV9-GFP-MBNL1Δ, AAV9-GFP or saline. **G**, Gene expression changes (adj p-value<0.05; |Log2FC|>1) in muscle of WT mice injected with either AAV9-GFP-MBNL1Δ or AAV9-GFP (upper panel) and differential expression of genes containing either CTGn repeat tracts (n≥7) or identified by CLIP as directs MBNL1 targets (lower panel).

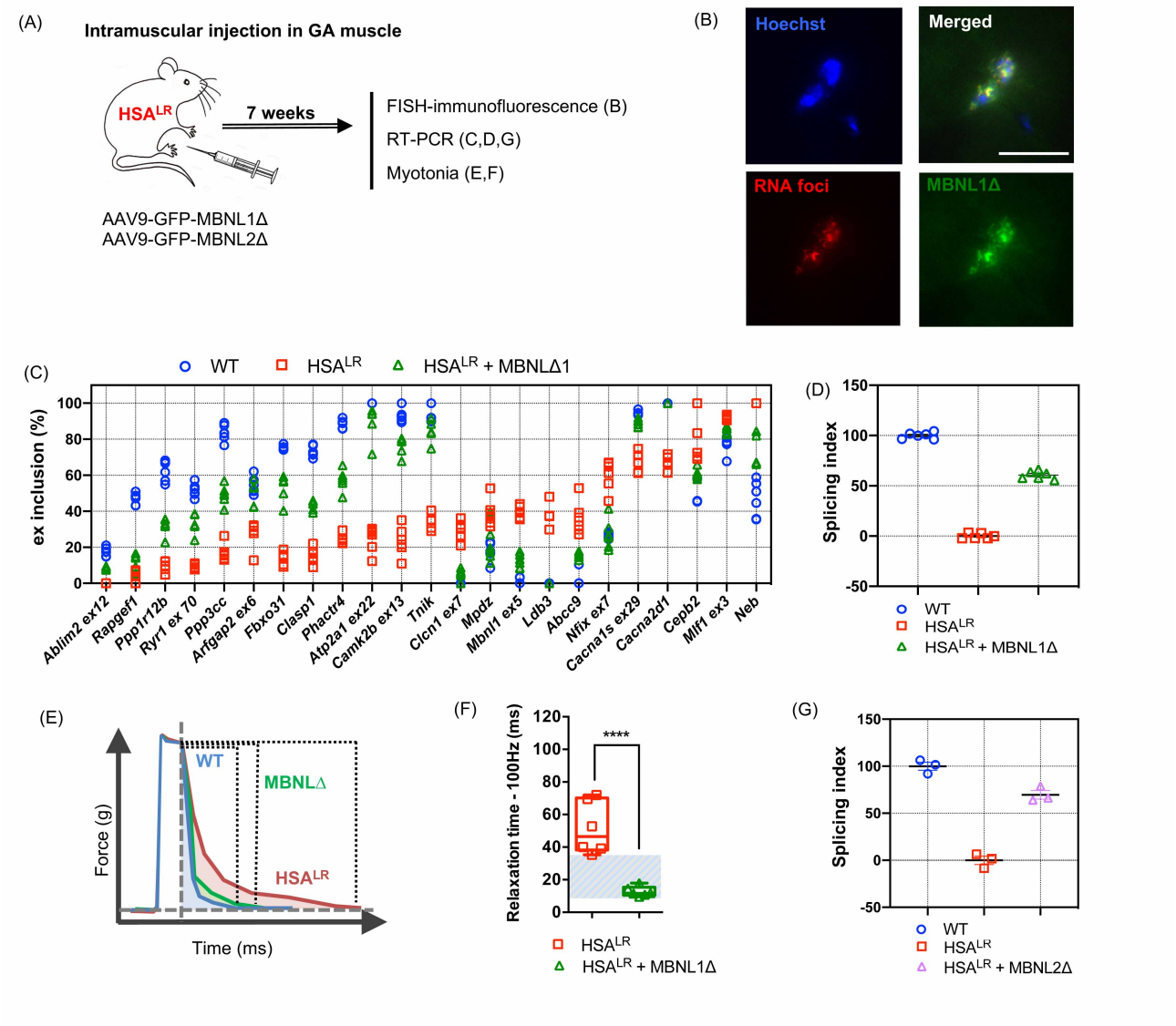

Fig. 5 Intramuscular injection of AAV-MBNL1Δ corrects splicing defects and myotonia in HSA^{LR} mice. **A**, Experimental design: *Gastrocnemius* (GA) muscles of HSA^{LR} mice injected with AAV9-GFP-MBNL1Δ or -MBNL2Δ vectors (1x10^{11} vg) for 7 weeks. Contralateral muscles received saline vehicle. **B**, Colocalization of GFP-MBNL1Δ with CUGexp-RNA foci in myonuclei of AAV9-GFP-MBNL1Δ treated HSA^{LR} mice visualized by combined RNA-FISH/immunofluorescence. CUGexp-RNA foci detected with a Cy3-CAG probe (red), GFP-MBNL1Δ using an anti-GFP antibody (green) and nuclei with Hoechst staining (blue). Scale bar: 10μm. **C**, Correction of 23 DM1-misspliced events regulated by MBNL1 in *GA* muscles of HSA^{LR} mice injected with AAV9-GFP-MBNL1Δ. **D**, Composite splicing index determined in HSA^{LR} *GA* muscles expressing MBNL1Δ (n=6). **E**, Illustrative representation of contractile properties and force development after *in situ* electric stimulation in muscle from WT, HSA^{LR} or MBNL1Δ-treated HSA^{LR} mice. Myotonia determined as the integrated area under the force/time curve during muscle relaxation. **F**, Relaxation time measurement in MBNL1Δ-treated HSA^{LR} muscles compared to contralateral saline-injected muscles (n=6). Data analyzed by unpaired Mann-Whitney Student's t-test (**$p < 0.01$). Relaxation time from WT mice represented by the blue area (n=17, two independent experiments). **G**, Composite splicing index determined in HSA^{LR} *GA* muscles expressing MBNL2Δ (n=3).

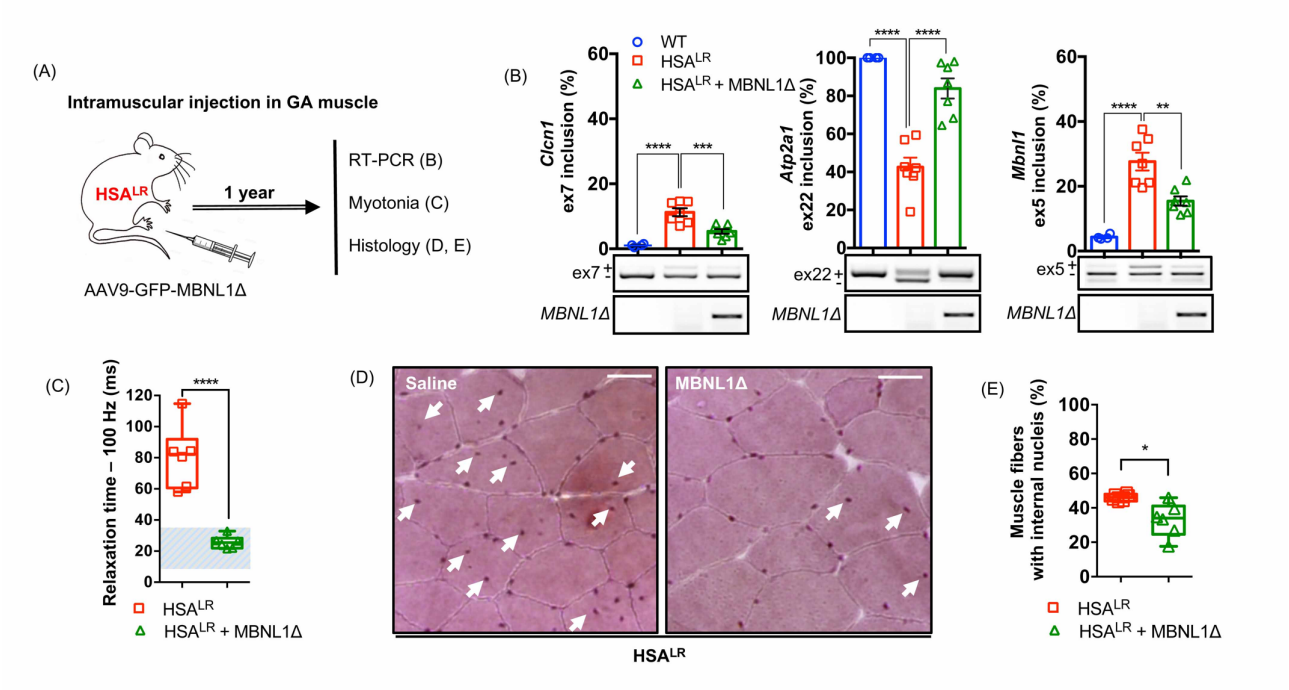

Fig. 6 l Long term correction of DM1-associated defects in MBNL1Δ-treated HSA^{LR} mice. A, Experimental design: *Gastrocnemius* muscles of 3 months-old HSA^{LR} mice injected with AAV9-GFP-MBNL1Δ vectors (1x10^{11} vg) for one year. Contralateral muscles received saline vehicle. **B**, Correction of *Clcn1 exon 7a, Atp2a1 exon 22* and *Mbnl1 exon 5* alternative splicing defects assessed by RT-PCR in MBNL1Δ-treated muscles of HSA^{LR} mice and compared to contralateral saline-injected muscles (n=7) and muscles from WT mice (n=3). Data analyzed by one-way ANOVA followed by Tukey's test (**$p < 0.01$, ***$p < 0.001$, ****$p < 0.0001$). **C**, Myotonia analysis in MBNL1Δ-treated HSA^{LR} muscles and saline-injected contralateral muscles (n=6). Data analyzed by unpaired Mann-Whitney Student's t-test (**$p < 0.01$). Relaxation time from WT mice represented by the blue area (n=17 mice, two independent experiments). **D**, Representative hematoxylin and eosin staining (HE) of AAV9-GFP-MBNL1Δ or saline injected HSA^{LR} *Gastrocnemius* muscles. Internalized nuclei within fibers were indicated by white arrows. **E**, Quantification of the number of fibers with internalized nuclei in HSA^{LR} *Gastrocnemius* muscles injected with AAV-GFP-MBNL1Δ compared to contralateral muscle injected with saline (n=6, average of 1400 fibers per muscles). Data analyzed by paired Student's *t*-test (*$p < 0.05$).

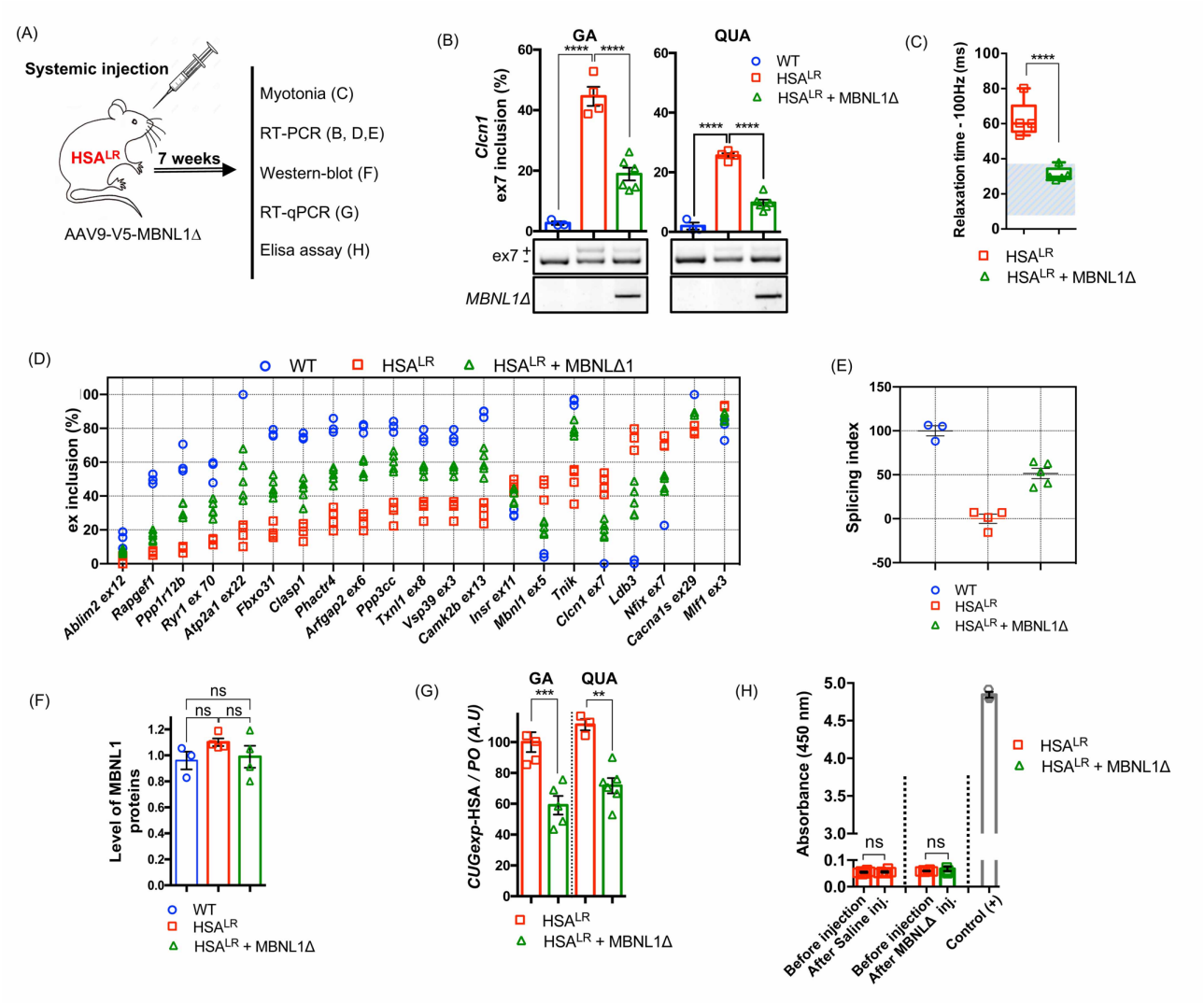

Fig. 7 l Systemic treatment with AAV-MBNL1Δ improves myotonia, splicing defects and decreases *CUGexp-RNA* levels in HSA^{LR} mice. A, Experimental design: three months-old HSA^{LR} mice systemically injected in retro-orbital sinus with AAV-V5-MBNL1Δ (9x10^{12} vg) or saline vehicle for 7 weeks. Three months-old WT FVB mice injected with saline vehicle. **B**, Myotonia analysis in *Gastrocnemius* muscles of MBNLΔ-treated or saline-injected HSA^{LR} mice (n=6). Data analyzed by unpaired Mann-Whitney Student's t-test (**p < 0.01). Relaxation time from WT mice represented by the blue area (n=17 mice, two independent experiments). **C**, Correction of *Clcn1 exon 7a* alternative splicing misregulation in *Gastrocnemius* (GA) and *Quadriceps* (QUA) muscles of HSA^{LR} mice following systemic MBNL1Δ treatment (n=6) compared to saline-injected HSA^{LR} (n=4) and WT mice (n=3). Data analyzed by one-way ANOVA followed by Tukey's test (****p < 0.0001). **D**, Correction of 23 DM1-misspliced events regulated by MBNL1 in *GA* muscles of MBNL1Δ treated-HSA^{LR} mice compare to saline injected-HSA^{LR} mice. **E**, Composite splicing index MBNL1 determined in *GA* muscles of MBNL1Δ treated-HSA^{LR} mice. **F**, Levels of MBNL1 proteins assessed by Western blot in GA muscles of MBNL1Δ-treated HSA^{LR} mice (n=4) and saline-injected HSA^{LR} or WT mice (n=3). Data analyzed by one-way ANOVA followed by Tukey's test (ns: no significant). **G**, Levels of *CUGexp-HSA* transcripts determined *by* quantitative RT-PCR in GA and QUA muscles of HSA^{LR} mice treated by MBNLΔ (n=4-6). Data analyzed by unpaired Mann-Whitney Student's t-test (*p<0.05, **p < 0.01). **H**, Detection of circulating immunoglobulins against MBNL1Δ by ELISA assay on sera collected before and 7 weeks after systemic administration of either AAV9-V5-MBNL1Δ or saline vehicle in HSA^{LR} mice (n=6).

Extended Data Fig. 1

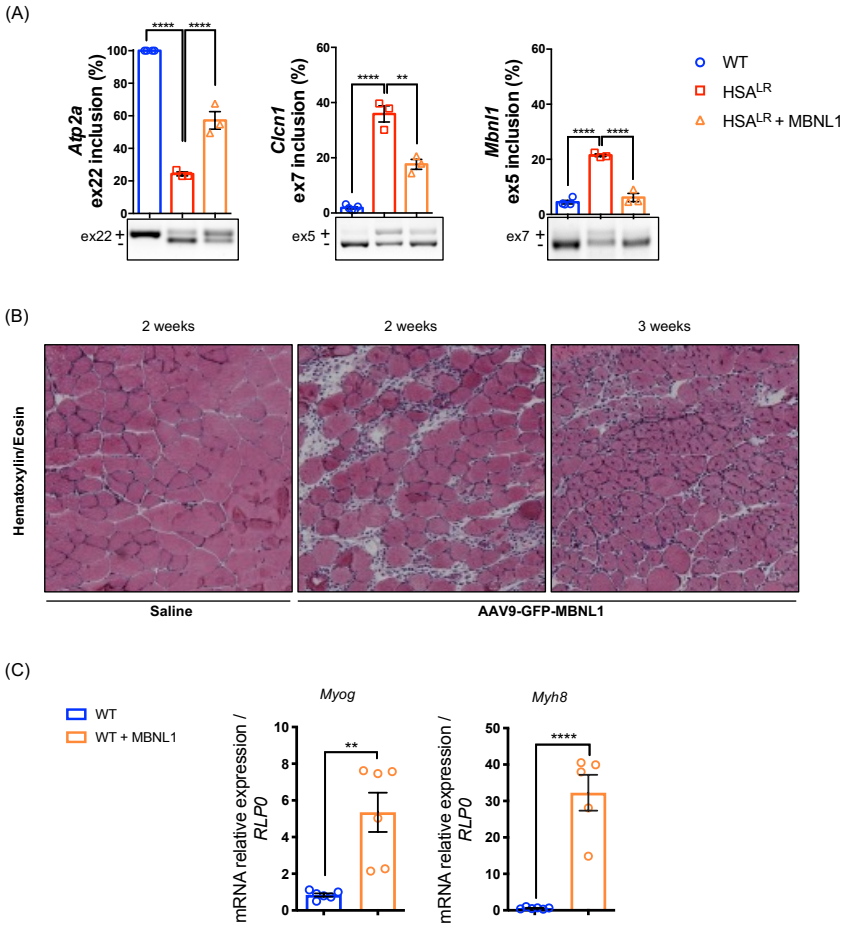

Extended Data Fig. 1 : Intramuscular injection of AAV-GFP-MBNL1 corrects splicing defects in HSA^{LR} mice but has deleterious effects in WT mice. (A) Correction of *Atp2a1 exon 22, Clcn1 exon 7a* and *Mbnl1 exon 5* alternative splicing assessed by RT-PCR in *Gastrocnemius* of HSA^{LR} mice after local intramuscular injection of AAV9-GFP-MBNL1 (1x10^{11} vg, n=3) and compared to saline vehicle-injected contralateral muscle or muscle from WT mice (n=4). Data analyzed by one-way ANOVA followed by Tukey's test (****p<0.0001). **(B)** Hematoxylin and Eosin (HE) staining performed on GA muscle sections of WT mice injected with AAV9-GFP-MBNL1 vectors (1x10 ^{11} vg) or saline for 2 or 3 weeks. **(C)** Expression of Myog and Myh8 measured by RT-qPCR in FVB muscles injected with AAV9-GFP-MBNL1 or saline for 2 weeks.

Extended Data Fig. 2

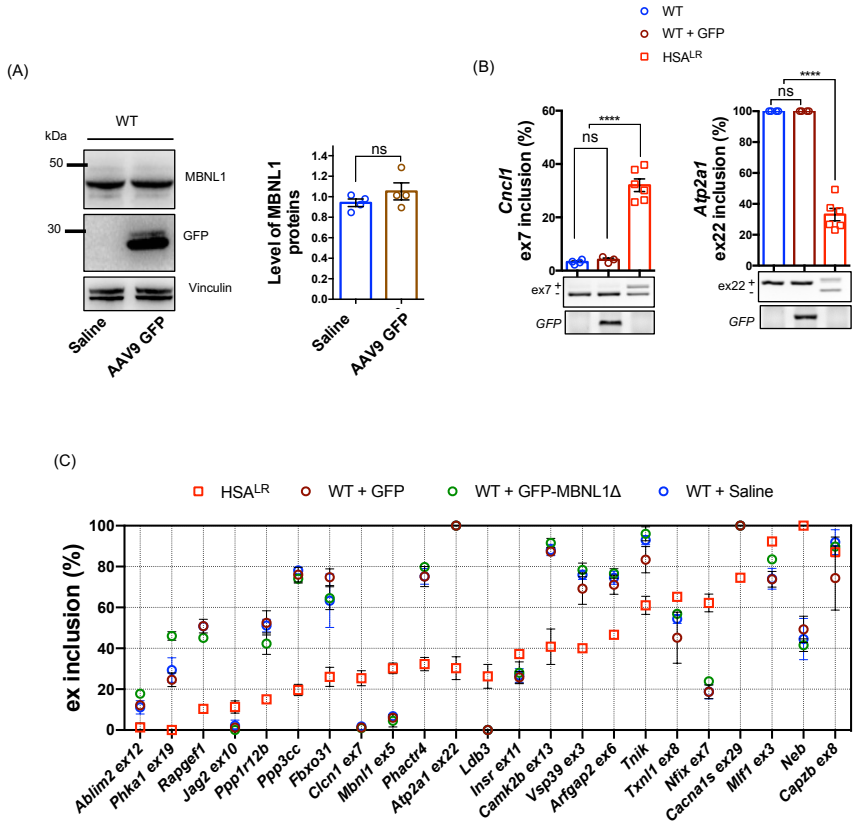

Extended Data Fig. 2 : Intramuscular injection of AAV-GFP has no effect on DM1 splicing events regulated by MBNL1. (**A**) Representative Western blot and quantification of MBNL1 protein level in WT *Gastrocnemius* muscles five weeks after intramuscular injection of AAV9-GFP ($1x10^{11}$ vg; n=4) or saline. Data analyzed by unpaired Student's t-test (ns: no significant). (**B)** Splicing profiles of *Clcn1 exon 7a* and *Atp2a1 exon 22* assessed by RT-PCR in WT mice five weeks after intramuscular injection of AAV9-GFP ($1x10^{11}$ vg) compared to saline vehicle-injected contralateral muscles or muscles form HSA^{LR} mice (n=3-6). Data analyzed by one-way ANOVA followed by Tukey's test (****$p < 0.0001$). (**C)** Modulation of 23 DM1-misspliced events regulated by MBNL1 in *GA* muscles of WT mice injected with AAV9-GFP-MBNL1Δ or AAV9-GFP compared to saline vehicle-injected contralateral muscles or muscles form HSA^{LR} mice (n=3).

Extended Data Fig. 3

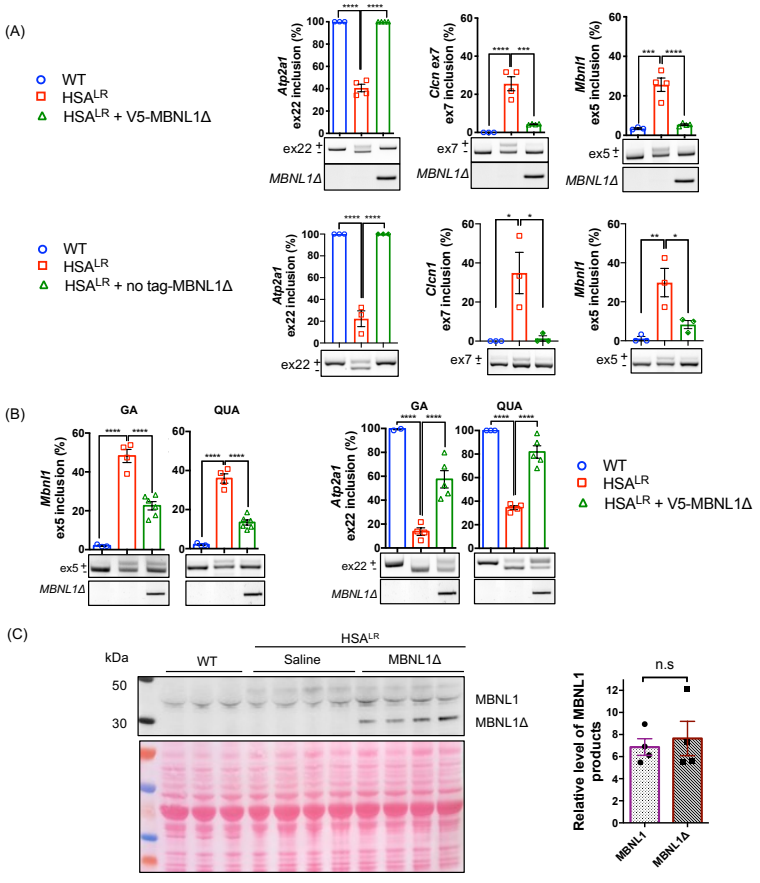

Extended Data Fig. 3 : Local and systemic administration of AAV-V5-MBNL1Δ corrects splicing defects in muscles of HSA^{LR} mice. (**A**) Correction of *Atp2a1 exon 22, Clcn1 exon 7a* and *Mbnl1 exon 5* alternative splicing assessed by RT-PCR in *Gastrocnemius* of HSA^{LR} mice after local intramuscular injection of AAV9-V5-MBNL1Δ (n=3-4, upper panel) or AAV9-MBNL1Δ (n=3, lower panel) and compared to saline vehicle-injected contralateral muscle or muscle from WT mice (n=4). Data analyzed by one-way ANOVA followed by Tukey's test (****p<0.0001). **(B)** Correction of *Atp2a1 exon 22* and *Mbnl1 exon 5* alternative splicing misregulation in *Gastrocnemius* (GA) and *Quadriceps* (QUA) muscles of HSA^{LR} mice following systemic MBNL1Δ treatment (n=5) compared to saline-injected HSA^{LR} (n=4) and WT mice (n=3). Data analyzed by one-way ANOVA followed by Tukey's test (****$p < 0.0001$). **(C)** Levels of MBNL1 proteins assessed by Western blot in GA muscles of MBNL1Δ-treated HSA^{LR} mice (n=4) and saline-injected HSA^{LR} or WT mice (n=3). Data analyzed by one-way ANOVA followed by Tukey's test (ns: no significant).

Extended Data Fig. 4

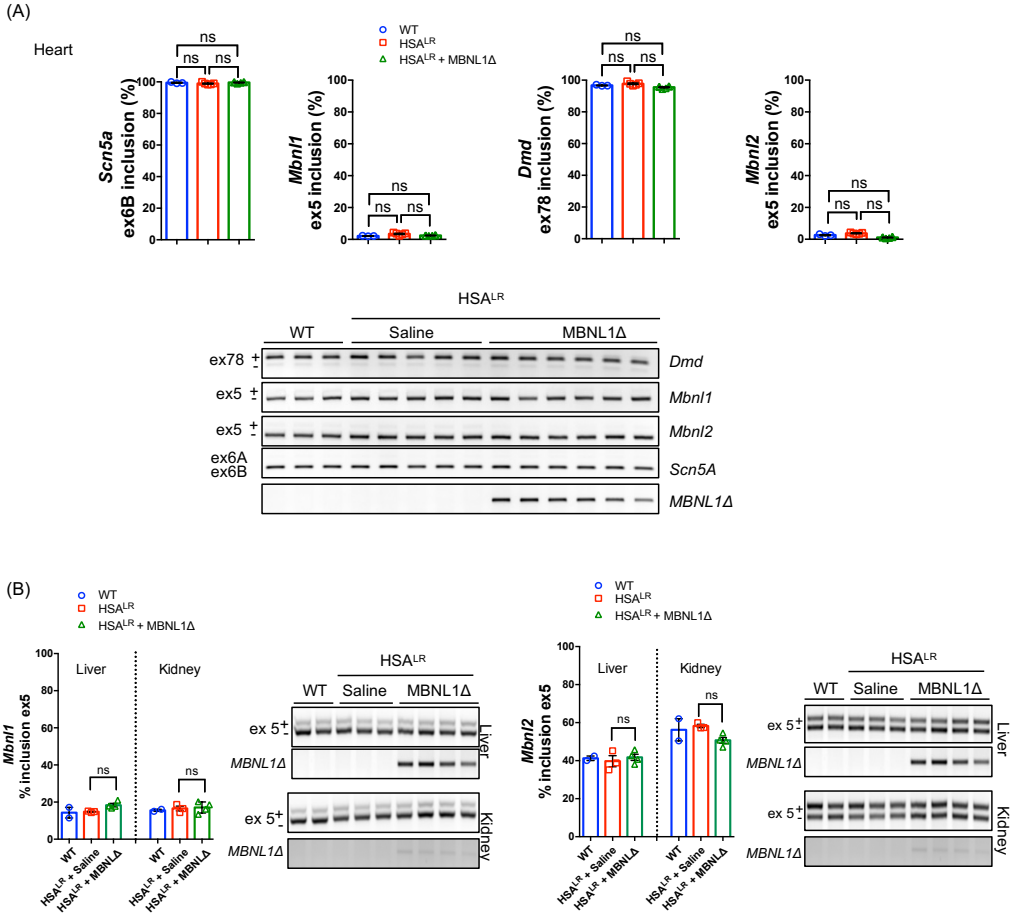

Extended Data Fig. 4: Analysis of DM1 splicing events in heart, liver and kidney of HSA^{LR} mice treated systemically with AAV-MBNL1Δ. (**A**) Splicing profiles of *Scn5a exon 6b, Mbnl1 exon 5, Dmd exon 78* and *Mbnl2 exon 5* in heart following systemic injection of AAV-V5-MBNLΔ or saline vehicle in HSA^{LR} mice (n=5-6) and compared to WT mice injected with saline vehicle (n=3) **(B)** Splicing profiles of *Mbnl1 exon 5* and *Mbnl2 exon 5* in kidney (K) and liver (L) assessed by RT-PCR following systemic injection of AAV-V5-MBNLΔ or saline vehicle in HSA^{LR} mice (n=3-4), and compared to WT mice injected with saline vehicle (n=2-3). Data analyzed by one-way ANOVA followed by Tukey's test (ns=no significant).

Contents

Supplementary Fig. 1. **MBNL1Δ has a reduced splicing activity but a similar CUG repeat binding affinity compare to MBNL1**

Supplementary Fig. 2. **MBNL1Δ corrects misregulated splicing events in DM1 muscle cells**

Supplementary Fig. 3. **Effects of MBNL1Δ treatment on major biological processes deregulated in DM1 cells.**

Supplementary Fig. 4. **MBNL1Δ does not alter the expression of MBNL compounds.**

Supplementary Fig. 5. **Correction of DM1 splicing defects by MBNL1Δ requires functional endogenous MBNL1 activity.**

Supplementary Fig. 6. **MBNL1Δ-decoy interferes with CUGexp-RNA foci dynamics.**

Supplementary Fig. 7. **Progressive correction of MBNL1-dependent splicing defects in DM1 cells following MBNL1Δ treatment.**

Supplementary Fig. 8. **Phase behavior of CUGexp-RNA/protein complexes**

Supplementary Fig. 9. **Top 20 biological processes in muscles of WT mice injected wither either AAV-GFP-MBNL1Δ or AAV-GFP.**

Supplementary Fig. 10. **MBNL1Δ colocalizes with CUGexp-RNA foci in myonuclei of treated HSA^{LR} muscles.**

Supplementary Fig. 11. **MBNL2Δ corrects DM1 splicing defects in HSA^{LR} mice.**

Supplementary Fig. 12. **Full gel/blot scans for supplementary figures.**

Supplementary Fig. 1

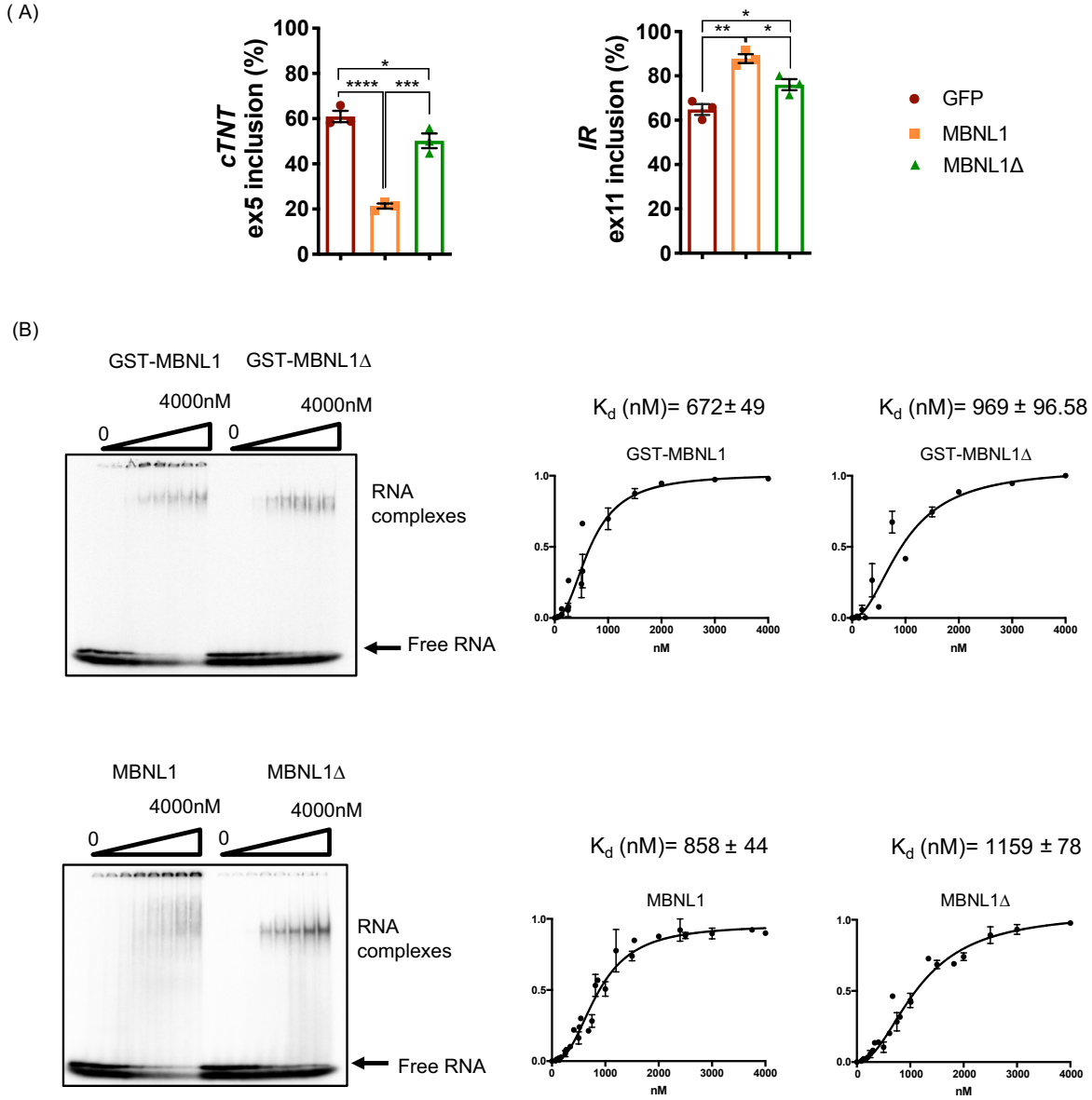

Supplementary Fig. 1
MBNL1Δ has a reduced splicing activity but a similar CUG repeat binding affinity compare to MBNL1. **(A)** RT-PCR analysis of splicing of *cTNT exon 5* and *IR exon 11* minigenes in Hela cells co-transfected with plasmids expressing GFP, GFP-MBNL1 or GFP-MBNL1Δ (n=3). Data analyzed by one-way ANOVA followed by Tukey's test (*$p < 0.05$, **$p < 0.01$, ***$p < 0.001$). **(B)** Representative mobility shift electrophoresis and CUGexp-binding curves used to assess the apparent dissociation constant ($K_d \pm$ s.d.) of double tagged GST-MBNL1-His and GST-MBNLΔ proteins (n=5) and MBNL1 and MBNL1Δ (n=7) proteins.

Supplementary Fig. 2

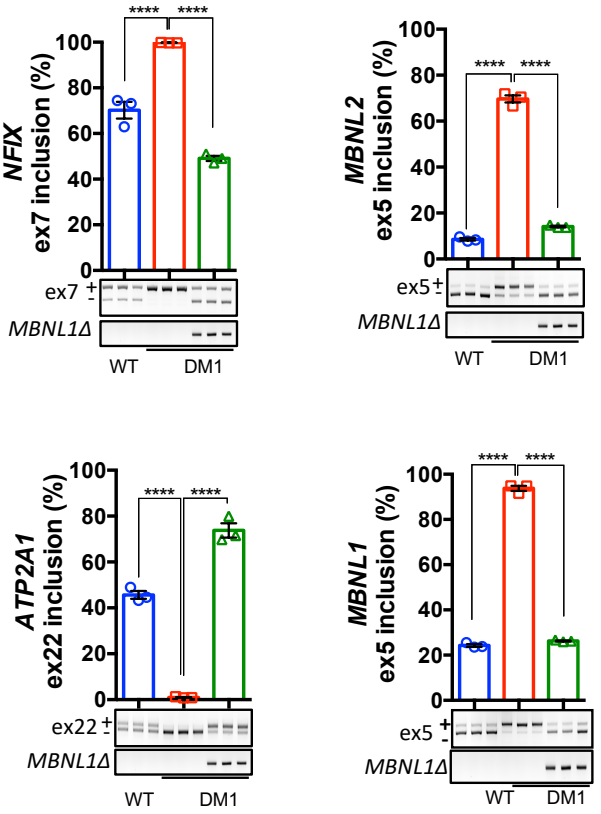

Supplementary Fig. 2
MBNL1Δ corrects misregulated splicing events in differentiated DM1 muscle cells. Correction of *NFIX exon 7, MBNL2 exon 5, ATP2A1 exon 22, MBNL2 exon 5* and *MBNL1 exon 5* alternative splicing assessed by RT-PCR in differentiated DM1 muscle cells expressing GFP-MBNL1Δ compared to differentiated non-treated DM1 and WT muscle cells (n=3). Data analyzed by one-way ANOVA followed by Tukey's test. (****$p < 0.0001$).

Supplementary Fig. 3

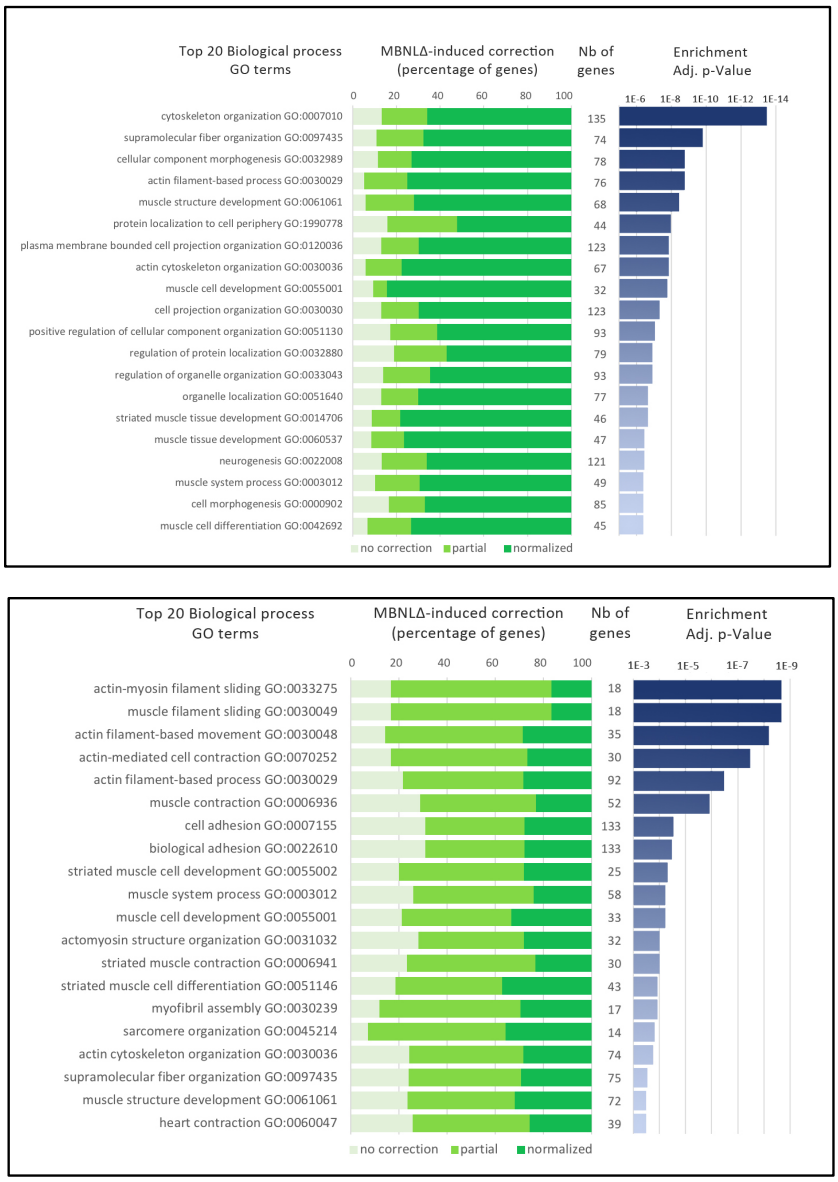

Supplementary Fig. 3
Effects of MBNL1Δ treatment on major biological processes deregulated in DM1 cells. List of the top 20 biological process identified by RNAseq following GO analysis of alternative splicing and gene expression in DM1 vs. WT cells. Both number of genes, P-value of each enriched term are represented in addition to the percentage of corrected, partially corrected or no corrected genes in MBNL1Δ-treated DM1 cells.

Supplementary Fig. 4

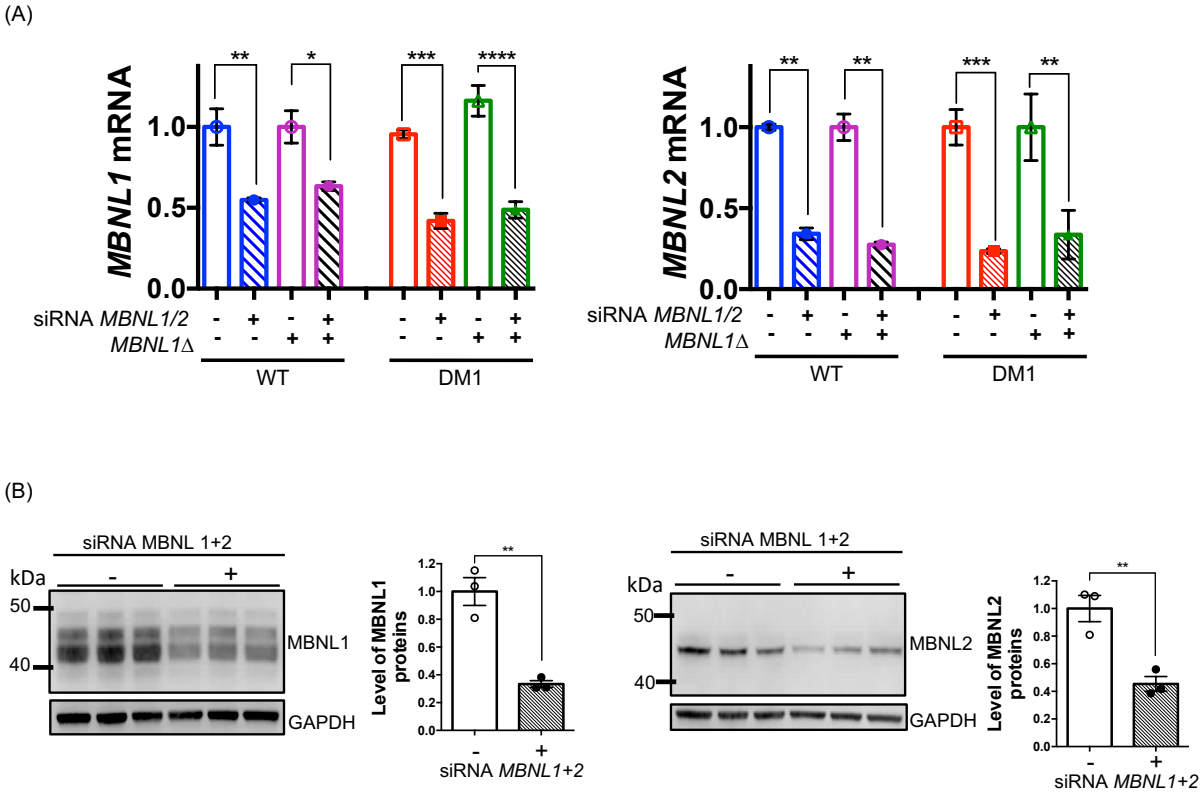

Supplementary Fig. 4
MBNL1Δ does not alter the expression of MBNL compounds. (**A**) Differentiated WT or DM1 muscles cells were transfected with siRNA directed against *MBNL1* and *MBNL2* mRNA at day 2 and GFP-MBNL1Δ was induced or not by doxycycline at day 3. Samples were analyzed at day 6. Levels of *MBNL1* and *MBNL2* mRNA determined by quantitative RT-PCR in WT, DM1 and MBNL1Δ-treated DM1 muscles cells (*n*=4). Data analyzed by one-way ANOVA followed by Tukey's test. (*$p < 0.05$, **$p < 0.01$, ***$p < 0.001$, ****$p < 0.0001$). (**B)** Levels of MBNL1 and MBNL2 protein determined by western blot in differentiated WT muscle cells (n=3). Data analyzed by unpaired Student t-test. (**$p < 0.01$).

Supplementary Fig. 5

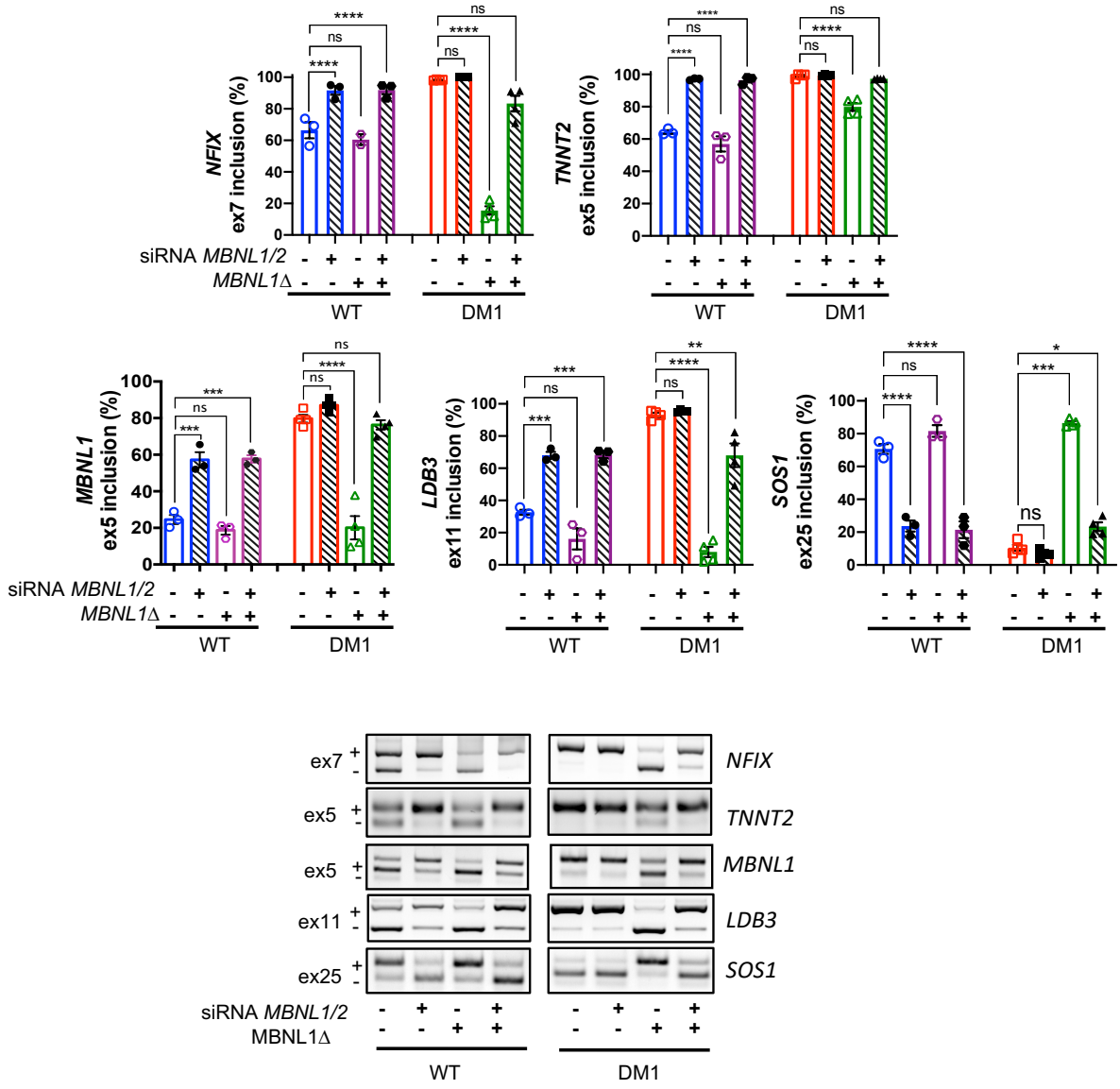

Supplementary Fig. 5
Correction of DM1 splicing defects by MBNL1Δ requires functional endogenous MBNL1 activity. Analysis of alternative of splicing changes of *NFIX exon 7, TNNT2 exon 5, MBNL1 exon 5*, *LDB3 exon* and *SOS1 exon 25* in 6-days differentiated WT or DM1 muscles cells transfected with or without siRNA directed against *MBNL1* and *MBNL2* mRNA at day 2 and expressing or not GFP-MBNL1Δ at day 3 (n=3-4). Data analyzed by one-way ANOVA followed by Tukey's test (*$p < 0.1$, ***$p < 0.001$, ****$p < 0.0001$).

Supplementary Fig. 6

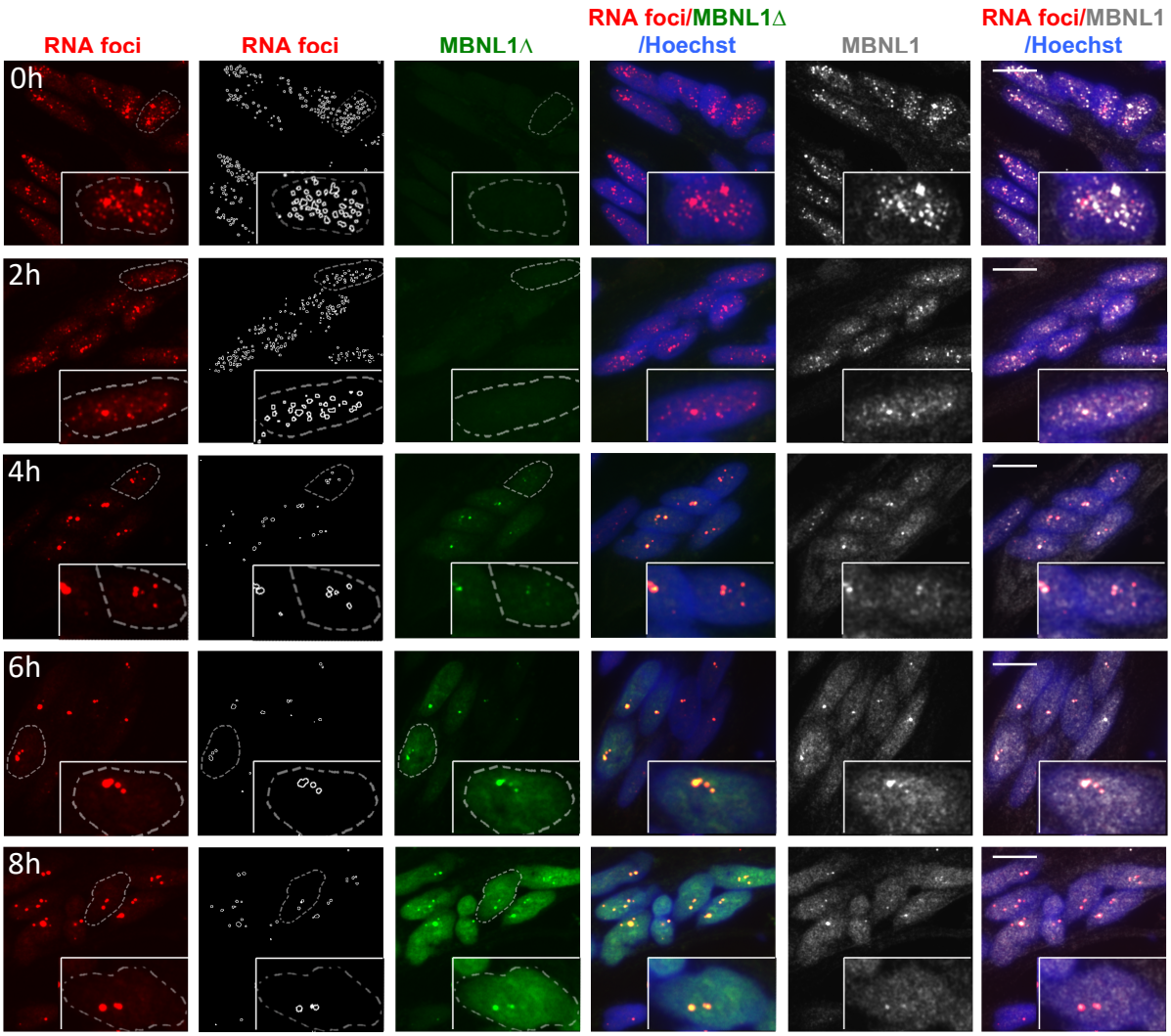

Supplementary Fig. 6
MBNL1Δ-decoy interferes with CUGexp-RNA foci dynamics. Representative RNA-FISH/Immunofluorescence images of differentiated DM1 muscle cells over a time-course from 2 to 8 hours after induction of GFP-MBNL1Δ expression compared to non-treated DM1 muscle cells. CUGexp-RNA foci detected with a Cy3-CAG probe (red), GFP-MBNL1Δ (green) endogenous MBNL1 with an antibody directed against the C-terminal part of the protein (grey) and nuclei with Hoechst staining (blue). RNA foci in the second panel from the left identified as white outlines on dark background by automated image analysis software. The nucleus perimeter represented by Dotted line in the enlarged picture. Scale bar: 10μm.

Supplementary Fig. 7

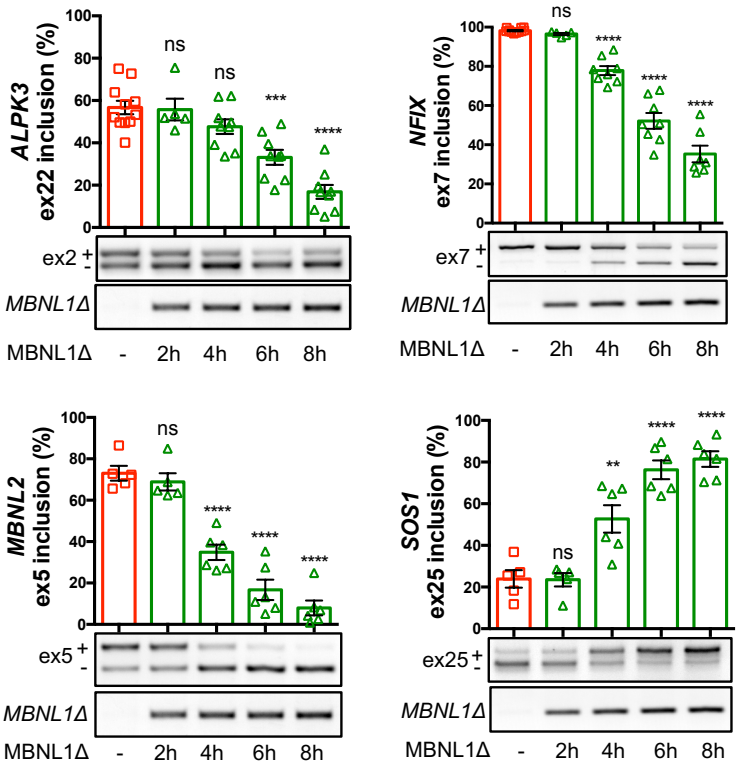

Supplementary Fig. 7
Progressive correction of MBNL1-dependent splicing defects in DM1 cells following MBNL1Δ treatment. RT-PCR analysis of splicing correction of *ALPK3 exon 2, NFIX exon 7, MBNL2 exon 5* and *SOS1 exon 25* following time course of MBNL1Δ treatment (n=5-9) compared to non-treated DM1 muscle cell (n=11). Data analyzed by one-way ANOVA followed by Tukey's test (**$p < 0.01$, ***$p < 0.001$, ****$p < 0.0001$, ns: no significant).

Supplementary Fig. 8

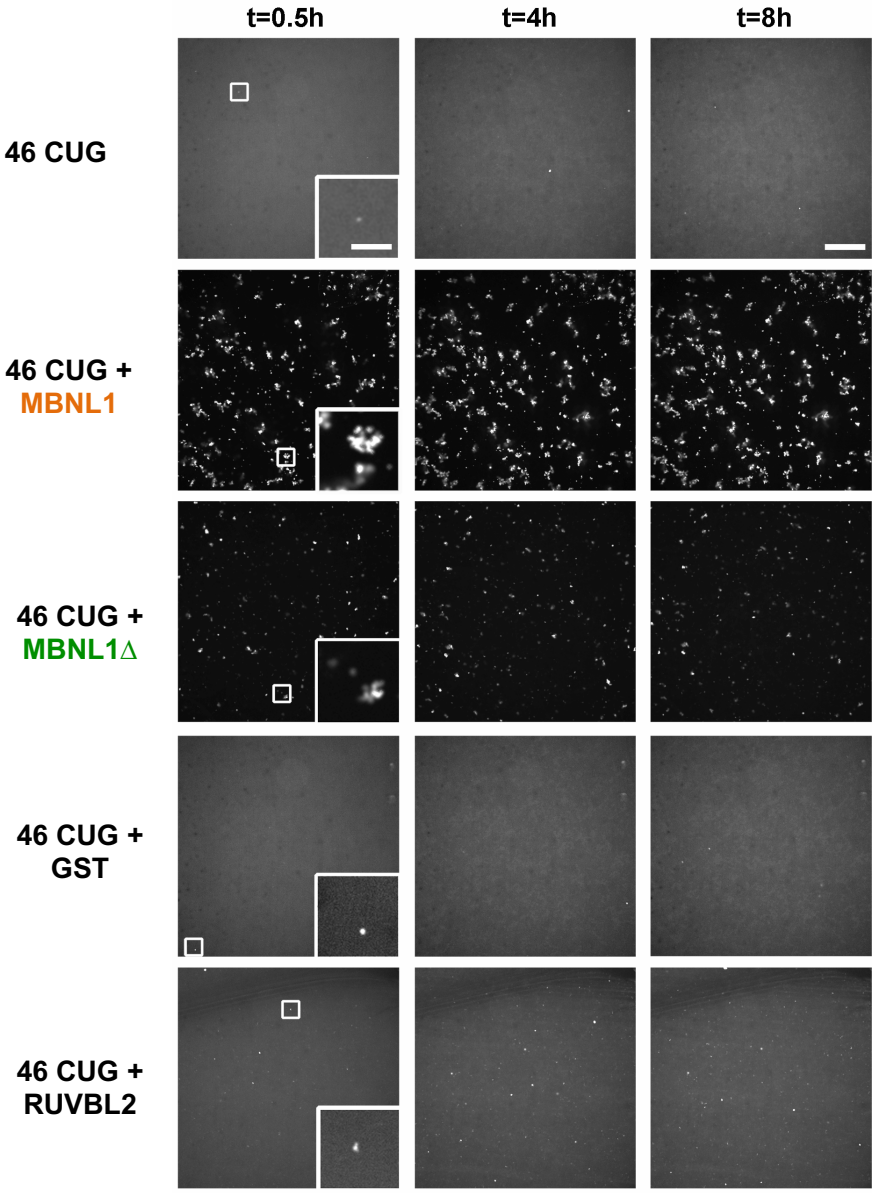

Supplementary Fig. 8
Phase behavior of CUGexp-RNA/protein complexes. Representative images of fluorescent RNA droplet formation in the absence or presence of MBNL1, MBNL1Δ, GST or RUVBL2 recombinant proteins at different time points. 2.5 mM of recombinant MBNL1, MBNL1Δ, GST or RUVBL2 were added to 500nM Cy3-CUG 46 in droplet formation buffer containing 100nM NaCl. Magnification 40x; Scale bar 50μm; Scale bar in insert 10μm.

Supplementary Fig. 9

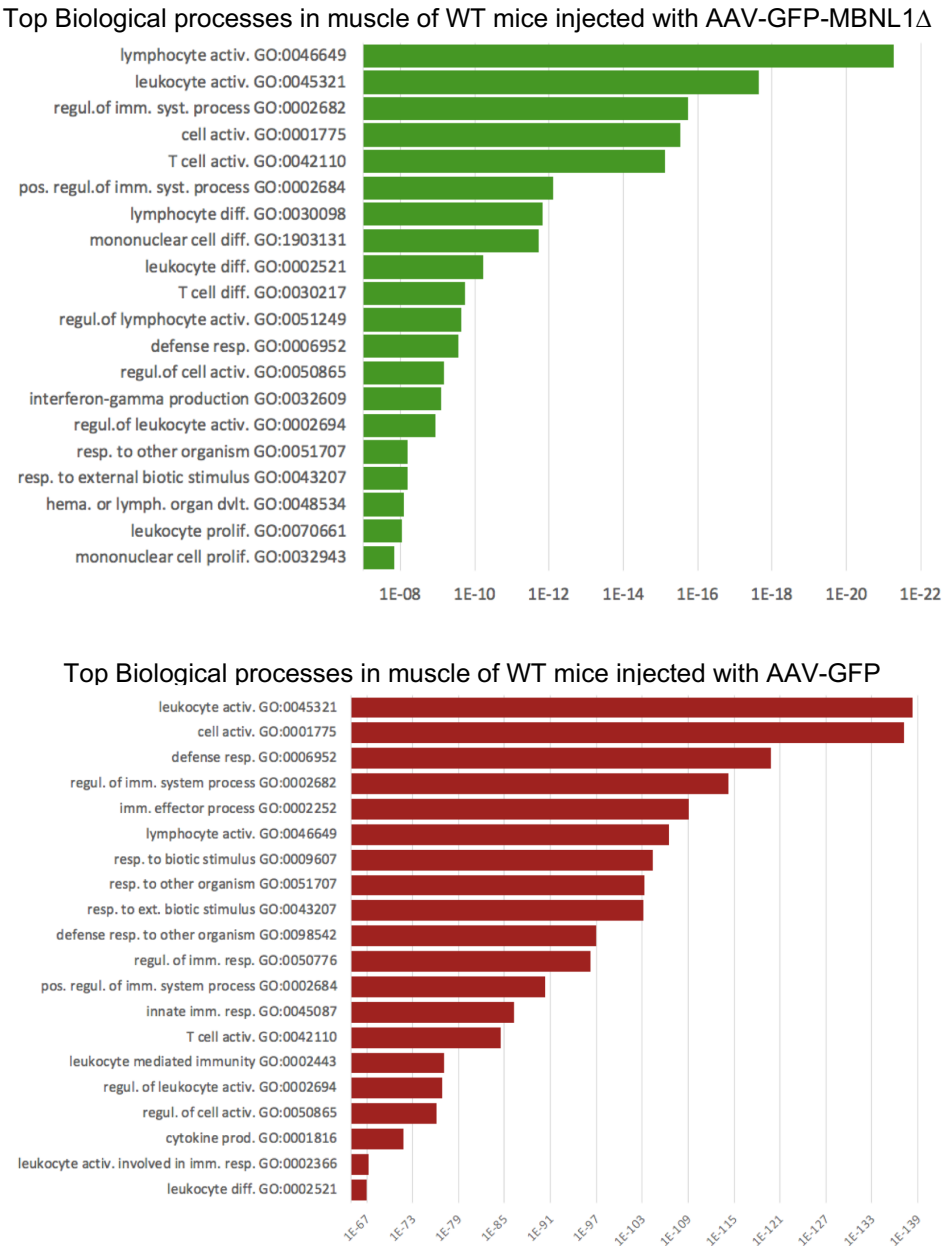

Supplementary Fig. 9
Top 20 biological processes in muscles of WT mice injected wither either AAV-GFP-MBNL1Δ or AAV-GFP.

Supplementary Fig. 10

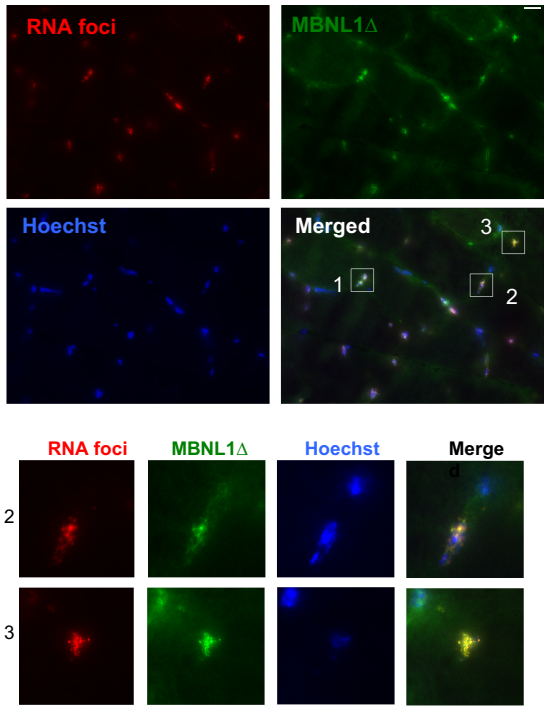

Supplementary Fig. 10
MBNL1Δ colocalizes with CUGexp-RNA foci in myonuclei of treated HSA^{LR} muscles. Combined RNA-FISH/immunofluorescence performed on *Gastrocnemius* cryosections of HSA^{LR} mice treated with AAV9-GFP-MBNLΔ. CUGexp-RNA foci detected with a Cy3-CAG probe (red), GFP-MBNLΔ using an anti-GFP antibody (green) and nuclei with Hoechst staining (blue). Upper panel: 20x magnification (scale bar: 50 μm). Lower panel: enlarged pictures (scale bar 10 μm). Note that enlarged picture 1 was included in Fig. 5 as panel B.

Supplementary Fig. 11

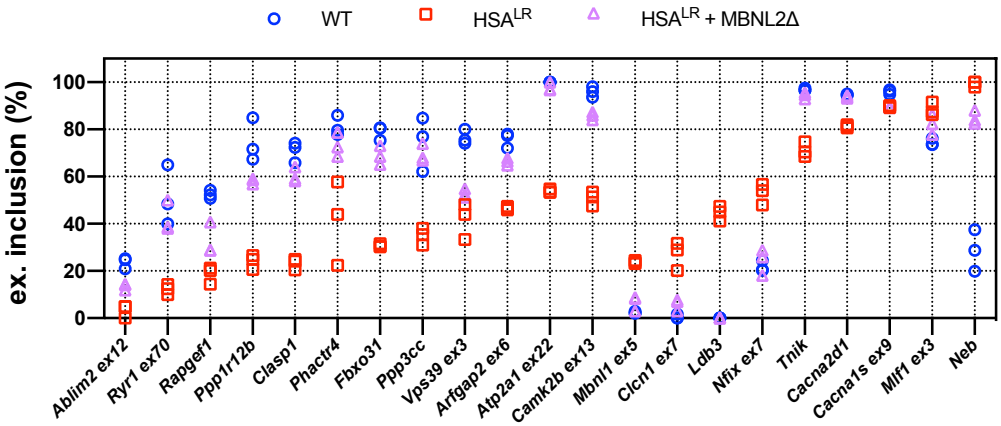

Supplementary Fig. 11.
MBNL2Δ corrects DM1 splicing defects in HSA^{LR} mice.
Correction of DM1-misspliced events regulated by MBNL1 in *GA* muscles of HSA^{LR} mice injected with AAV9-GFP-MBNL2Δ (n=3).

Supplementary Fig. 12. Full gel/blot scans for the supplementary figures.

Supplementary Fig. 2A

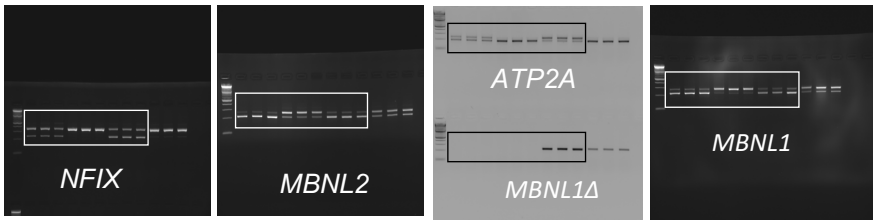

Supplementary Fig. 4A

Left panel

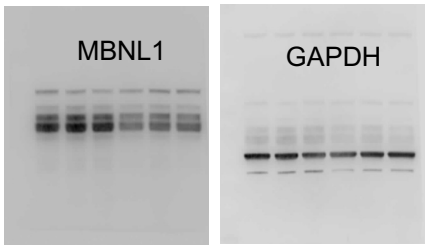

Right panel

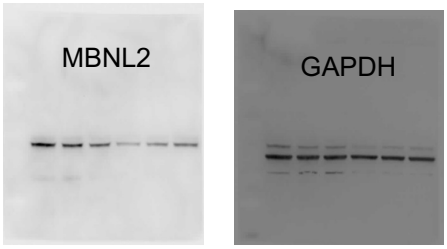

Supplementary figure 5

All images have undergone a horizontally symetric rotation for figures

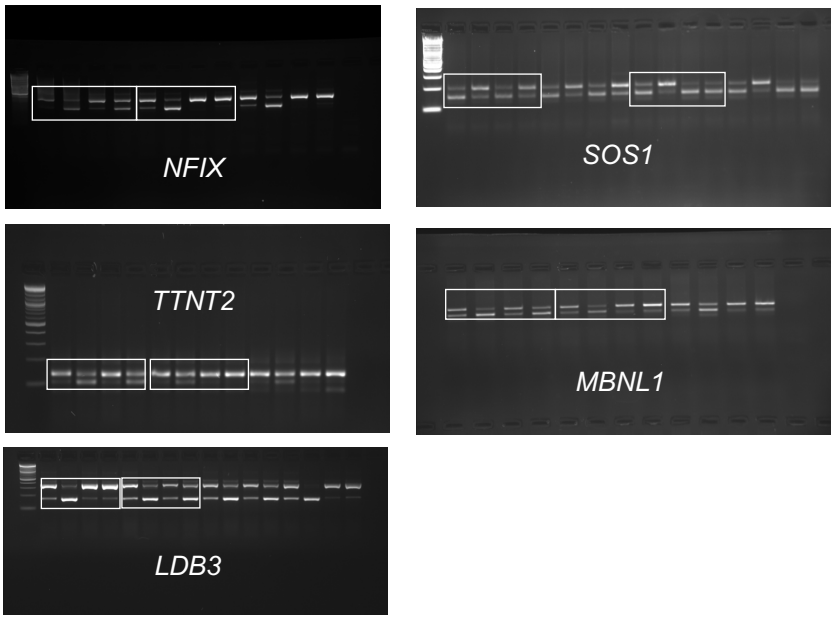

Supplementary Fig. 7